

Numerical study on the influence of acoustic natural frequencies on the dynamic behaviour of submerged and confined disk-like structures

Matias Bossio, David Valentín, Alexandre Presas, David Ramos Martin, Eduard Egusquiza, Carme Valero, Mònica Egusquiza

Centre de Diagnòstic Industrial i Fluidodinàmica, Universitat Politècnica de Catalunya, Av. Diagonal, 647, ETSEIB, Pab. D+I, 08028 Barcelona, Spain.

ABSTRACT

The dynamic response of disks has been deeply studied in the last years given that their dynamic characteristics present similarities with more complex disk-like structures used in real engineering applications, such as hydraulic turbine runners. Because of disk-like structures could present fatigue damage or critical failures as a result of resonance conditions, it is of paramount importance to determine their natural frequencies.

The dynamic response of disk-like structures is heavily affected by the added mass effect when they are surrounded by a heavy fluid. This added mass is greatly affected by the proximity of walls. Furthermore, the surrounding fluid cavity has its own natural frequencies and mode shapes, called acoustic natural frequencies and acoustic mode-shapes. All studies of submerged and confined disks have been carried out considering that the acoustic natural frequencies of the surrounding fluid cavity are much higher than the natural frequencies of the disk, so they do not affect each other. However, in some cases the acoustic natural frequencies are close to the natural frequencies of the submerged structure, which can be affected considerably. This case has not been deeply discussed yet.

In this paper, the influence of the acoustic natural frequencies of a cylindrical fluid cavity on the natural frequencies of a disk has been analysed numerically. First, the effect of the added mass of the fluid has been estimated when the acoustic natural frequencies of the fluid cavity are much higher than the natural frequencies of the disk. For this case, different geometrical and material parameters have been considered. Then, the parameters that affect the acoustical natural frequencies of the fluid cavity have been identified. Finally, the case with acoustic natural frequencies close to the structural natural frequencies is studied in detail and the affectation between both is discussed. All the results presented in this paper have been dimensionless in order to be used for a wide range of disk-like structures.

Therefore, with this study it is possible to identify for which conditions the dynamic response of a generic disk-like structure will be affected by the acoustic natural frequencies of its surrounding fluid cylindrical cavity.

Keywords

Disk-like structure, Acoustic frequencies, Natural frequencies, Submerged disk, Added mass, Speed of sound

1 Introduction

To determine the natural frequencies of disk-like structures could avoid resonance conditions that may cause fatigue damage or critical failure. This is of paramount importance in actual engineering applications, as is the case of hydraulic runners. Some types of hydraulic runners are disk-like structures which are submerged and confined in a heavy fluid and their dynamic response are greatly affected by the boundary conditions (Valentín et al., 2014). The fluid density, the value of the speed of sound in the fluid medium and geometrical dimensions have to be considered in order to understand the effect of those parameters on the natural frequencies and mode-shapes. Due to the similarity on the mode-shapes between the disk and the more complex disk-like structures such as hydraulic runners (Egusquiza et al., 2012; Huang, 2011; Huang et al., 2013a; Liang et al., 2007; Presas et al., 2012; Tanaka, 2011), the dynamic response of disks has been deeply studied in the last years.

Disk-like structures have been studied in many cases surrounded by low density fluid such as air. Blevins (2001) conducted several studies of a wide range of structures on air, such as plates and annular plates with different boundary conditions, in order to analytically determine the natural frequencies and mode-shapes. In this study and others (Bauer and Eidel, 2007; Campbell, 1924; Heo and Chung, 2004; Lamb and Southwell, 1921; Southwell, 1922) it is concluded that the effect of the low densities surrounding fluids in natural frequencies and mode-shapes of the analysed structure can be neglected.

On the other hand, if the structure is surrounded by heavy fluid, its dynamic response is drastically affected. This effect is known as added mass effect, and it has been extensively used to calculate the natural frequencies of disk-like structures surrounded by heavy fluids such as water. Lindholm et al. (1962), Kwak (1991), Amabili and Kwak (1996), and Meyerhoff (1970) conducted experimental and numerical investigations in circular and rectangular plates in contact with water and they predicted the influence of the surrounding fluid on the dynamic response of the structure. Similarly, several studies have dealt with more complex structures. Rodriguez et al. (2006) carried out an experimental modal analysis of a Francis turbine in still water, showing a significant effect of the added mass effect in the natural frequencies. Also Liang et al. (2007) and Liang and Wang (2003) conducted a numerical simulation using finite element method (FEM) in order to analyse the influence of surrounding water in a turbine runner. According to these studies, the added mass effect reduces the natural frequencies of the submerged structure compared to those ones in air.

When the structure is bounded by rigid walls the added mass effect is even more important, being more interesting the effect of the small gaps. Plenty of studies of vibrating structures submerged and near a rigid wall were carried out (Askari et al., 2013; Harrison et al., 2007; Kubota and Ohashi, 1991; Kubota and Suzuki, 1984; Naik et al., 2003; Presas et al., 2016; Rodriguez et al., 2012; Valentín et al., 2014). All these studies conclude that the distance disk-wall has a great influence on the added mass effect, i.e. the natural frequencies decreased when the disk is close to a rigid surface. However, these studies only investigated the natural frequencies of the structure but without considering the dynamic response of the surrounding fluid cavity, which for certain conditions may affect the dynamic response of the structure itself.

A fluid cavity presents acoustic natural frequencies with corresponding mode-shapes, which are known as acoustic modes. Blevins (2001) investigated analytically the acoustic natural frequencies and acoustic modes for a wide range of cavities. These studies showed that the values of the acoustic natural frequencies are influenced by the geometrical parameters of the cavity as well as the fluid speed of sound. In the experimental domain, Graf et al. (2014) and Rossetto et al. (2001) conducted experimental and analytical modal analysis on a pipe and a cavity respectively, both of them analysing their eigenmodes. Nieter and Singh (1982) by means of an accelerometer and a microphone, developed an experimental method in order to obtain acoustic natural frequencies and modes for acoustics ducts. Several studies were carried out in order to predict the acoustic modes in aerospace industries, more precisely on ducted flows, (Dowling and Stow, 2003; Jourdain et al., 2013; Kousen, 1999; Scholl et al., 1998). Nevertheless, the interaction between

structural and acoustical part, i.e. the case of a submerged structure and confined with structural natural frequencies close to acoustic natural frequencies of the cavity has not been deeply discussed yet.

In this paper, the acoustical and structural natural frequencies of a flexible disk enclosed in a rigid cylindrical cavity and surrounded by a heavy fluid have been analysed in detail. By means of coupled simulations, the influence of the acoustic natural frequencies on the dynamic response of the disk has been evaluated. The parameters that have a great influence on the structural and acoustic natural frequencies have been identified and the results are presented as a function of those. With the results presented in this paper, the natural frequencies of a wide range of disks submerged in a different kind of fluids with different confining configurations can be obtained and, moreover, it can be also determined if the acoustical natural frequencies of the fluid cavity have any influence on the structural dynamic response of the flexible disk.

Nomenclature			
B	Matrix of gradient components	j	Nodal circles
C_f	Acoustic fluid damping matrix	k	Cross sections
C_s	Structural damping matrix	K_f	Acoustic fluid stiffness matrix
c	Speed of sound [m/s]	K_s	Structural stiffness matrix
c_0	Maximum speed of sound [m/s]	L	Laplacian factor
D	Disk diameter [m]	M_f	Acoustic mass matrix
D_{cav}	Cavity diameter [m]	M_s	Structural mass matrix
$D_{cav,base}$	Cavity diameter (Base case). [m]	m	Slope (acoustic mode-shapes)
E	Young modulus [N/m ²]	N_p	Element shape function for pressure
F_f	Load applied on the fluid elements	N_u	Element shape function for displacement
F_s	Applied load vector	n	Normal vector to s
F_{fs}	Fluid force (Coupled system)	p	Dynamic fluid pressure
F_{sf}	Structure force (Coupled system)	R	Area associated with each node (Coupled system)
f_{air}	Structural natural frequency in air. [Hz]	r_{cav}	Cavity radius [m]
f_{cav}	Acoustic natural frequency of the cavity. [Hz]	r_{int}	Interior radio [m]
$f_{cav,base}$	Acoustic natural frequency of the cavity (Base case). [Hz]	s	Interface surface of the cavity
f_f	Structural natural frequency. Submerged disk. c variable. [Hz]	u	Nodal displacement
$f_{f,c=\infty}$	Structural natural frequency. Submerged disk. $c = \infty$. [Hz]	V	Volume
G	Radial gap [m]	Z	Coordinate
H_{down}	Lower fluid distance [m]	<i>Percentage calculations</i>	
H_{tot}	Cavity height [m]	δ (%)	Difference between simulation and theory (structural frequencies)
H_{up}	Upper fluid distance [m]	φ (%)	Influence of the density ratio
		$\Delta_{no\ disk-disk}$ (%)	Difference between acoustic frequencies (without disk-with disk)

h_D	Disk thickness [m]	Δ_{sim-th} (%)	Difference between simulation and theory (acoustic frequencies)
i	Nodal diameters	<i>Acronyms</i>	
<i>Greek letters</i>		CPU	Central processing unit
λ	Correction factor (gap)	FEM	Finite Element Modeller
λ_{ik}	Tabulated parameter	FSI	Fluid-Structure Interaction
ν	Poisson's ratio		
ρ_f	Fluid density [kg/m ³]		
ρ_0	Fluid density [kg/m ³]		
ρ_D	Disk material density [kg/m ³]		
ψ	Correction factor (Density ratio).		

2 Numerical model

In this section the numerical equations that define the dynamic response of a structure inside a fluid domain are described. For this purpose, the structural and fluid part are firstly considered separately and then the coupling between both systems is analysed.

2.1 Dynamic behaviour of structure vibrating in vacuum.

The dynamic behaviour of a body vibrating in vacuum, can be described as (Liang et al., 2007):

$$[M_s]\{\ddot{u}\} + [C_s]\{\dot{u}\} + [K_s]\{u\} = \{F_s\} \quad (1)$$

where $[M_s]$ is the structural mass matrix, $[C_s]$ is the structural damping matrix, $[K_s]$ is the structural stiffness matrix, $\{F_s\}$ is the applied load vector and $\{u\}$ is the nodal displacement vector. Natural frequencies structure can be calculated then assuming $\{F_s\} = 0$, and transforming Eq. (1) in the frequency domain.

2.2 Dynamic behaviour of an acoustic cavity

The dynamic behaviour of an acoustic cavity can be analysed considering the dynamic pressure for each fluid element $\{p\}$ (see more details in Rodriguez et al. (2012) and Huang et al. (2013b)).

$$[M_f]\{\ddot{p}\} + [C_f]\{\dot{p}\} + [K_f]\{p\} = \{F_f\} \quad (2)$$

Where

$$[M_f] = 1/c^2 \int_{vol} \{N_p\}\{N_p\}^T dV, \quad (3)$$

$$[C_f] = \beta/c \int_s \{N_p\}\{N_p\}^T dS, \quad (4)$$

$$[K_f] = \int_{vol} \{B\}\{B\}^T dV, \quad (5)$$

$[M_f]$ is the acoustic mass matrix, $\{N_p\}$ is the element shape function for pressure and vol is the volume domain of the cavity. $[C_f]$ is the acoustic fluid damping matrix, β is the non-dimensional boundary absorption coefficient, which is defined as $\beta = \gamma/\rho_0 c$. γ is the characteristic impedance of the material at the boundary, ρ_0 the fluid density and c is the speed of sound in the fluid medium. The interface surface of the cavity is defined as s . $[K_f]$ is the acoustic fluid stiffness matrix, $[B] = \{L\}\{N_p\}^T$ where $\{L\}$ is the Laplacian vector and $\{F_f\}$ is the load applied on the fluid elements.

Natural frequencies of the acoustic cavity can be obtained assuming $\{F_f\}=0$ and transforming Eq. (2) in the frequency domain.

2.3 Dynamic behaviour of fluid-structure coupling.

When a structure is in contact with an acoustic cavity (in contact by one of its surfaces or totally submerged) both systems are coupled. In this case the structural equations of the coupled system can be written using Eq. (1) and Eq. (2).

$$\left. \begin{aligned} [M_s]\{\ddot{u}\} + [C_s]\{\dot{u}\} + [K_s]\{u\} &= \{F_s\} + \{F_{fs}\} \\ [M_f]\{\ddot{p}\} + [C_f]\{\dot{p}\} + [K_f]\{p\} &= \{F_f\} + \{F_{sf}\} \end{aligned} \right\} \quad (6)$$

Where $\{F_{fs}\}$ is the force that the fluid exerts on the structure due to the structure motion and $\{F_{sf}\}$ the force that the structure motion produces on the fluid. $\{F_{fs}\}$ and $\{F_{sf}\}$ can be obtained respectively as:

$$\{F_{fs}\} = \int_s \{N_u\}\{N_p\}^T \{n\} dS \cdot p = R \cdot p \quad (7)$$

$$\{F_{sf}\} = -\rho_0 [R]^T \{\ddot{u}\} \quad (8)$$

Where $\{N_u\}$ is the element shape function for displacement and $[R]$ represents the area associated with each node on the interface, which is defined as:

$$[R] = \int_s \{N_u\}\{N_p\}^T \{n\} dS \quad (9)$$

Where $\{n\}$ is the normal vector to s .

In order to calculate the natural frequencies, the damping can be neglected (considering a slightly damped system). By using Eq. (6) and the definitions for $\{F_{fs}\}$ (7) and $\{F_{sf}\}$ (8), taking $\{F_s\} = 0$ and $\{F_f\} = 0$, the finite element matrix equations to calculate the natural frequencies of both structure and fluid parts coupled are written as:

$$\left. \begin{aligned} [M_s]\ddot{u} + [K_s]u &= [R]p \\ [M_f]\ddot{p} + [K_f]p &= -\rho_0 [R]^T \ddot{u} \end{aligned} \right\} \quad (10)$$

Transforming Eq. (10) in the frequency domain

$$\left. \begin{aligned} [-[M_s]\omega^2 + [K_s]]u &= [R]p \\ [-[M_f]\omega^2 + [K_f]]p &= \rho_0 [R]^T \omega^2 u \end{aligned} \right\} \quad (11)$$

Now p can be isolated and therefore the structural part from Eq. (11) becomes:

$$\left[\left([-M_s] - \rho_0 [R] [-M_f \omega^2 + K_f]^{-1} [R]^T \right) \omega^2 + K_s \right] u = 0 \quad (12)$$

2.4 Speed of sound influence

In this section, the influence of the speed of sound of the fluid on the structural natural frequencies is qualitatively explained based on Eq. (12). When the speed of sound tends to infinite, the acoustic mass matrix tends to zero. Therefore Eq. (12) can be written as:

$$\left[\left([-M_s] - \rho_0 [R] [K_f]^{-1} [R]^T \right) \omega^2 + K_s \right] u = 0 \quad (13)$$

Solving the Eq. (13), the structural natural frequencies of the coupled system when the speed of sound tends to infinite can be calculated. In this situation the term $[R] [-K_f]^{-1} \rho_0 [R]^T$, which is directly added to $[M_s]$, can be considered as fluid added mass on the structural part (Amabili and Kwak, 1996; Kubota and Suzuki, 1984). Figure 1a shows qualitatively this situation

For $c < \infty$, the acoustic mass matrix becomes $[M_f] \neq 0$. In this case Eq. (12) defines the structural natural frequencies. As one can see, the fluid added mass of the structural part comprises now the acoustic mass matrix and the fluid stiffness matrix. Considering the situation of $0 \ll c$ so that the acoustic natural frequencies are much higher than the structural frequencies (Figure 1b), it can be seen that the influence on the structural natural frequency of this new term, $[M_f]$, is almost negligible.

Reducing the speed of sound, M_f becomes more significant on the fluid added mass term. In this case (Figure 1c), $[M_f]$, has a relevant contribution on the fluid added mass (increasing this term) and therefore the structural natural frequencies start to decrease compared with the previous case.

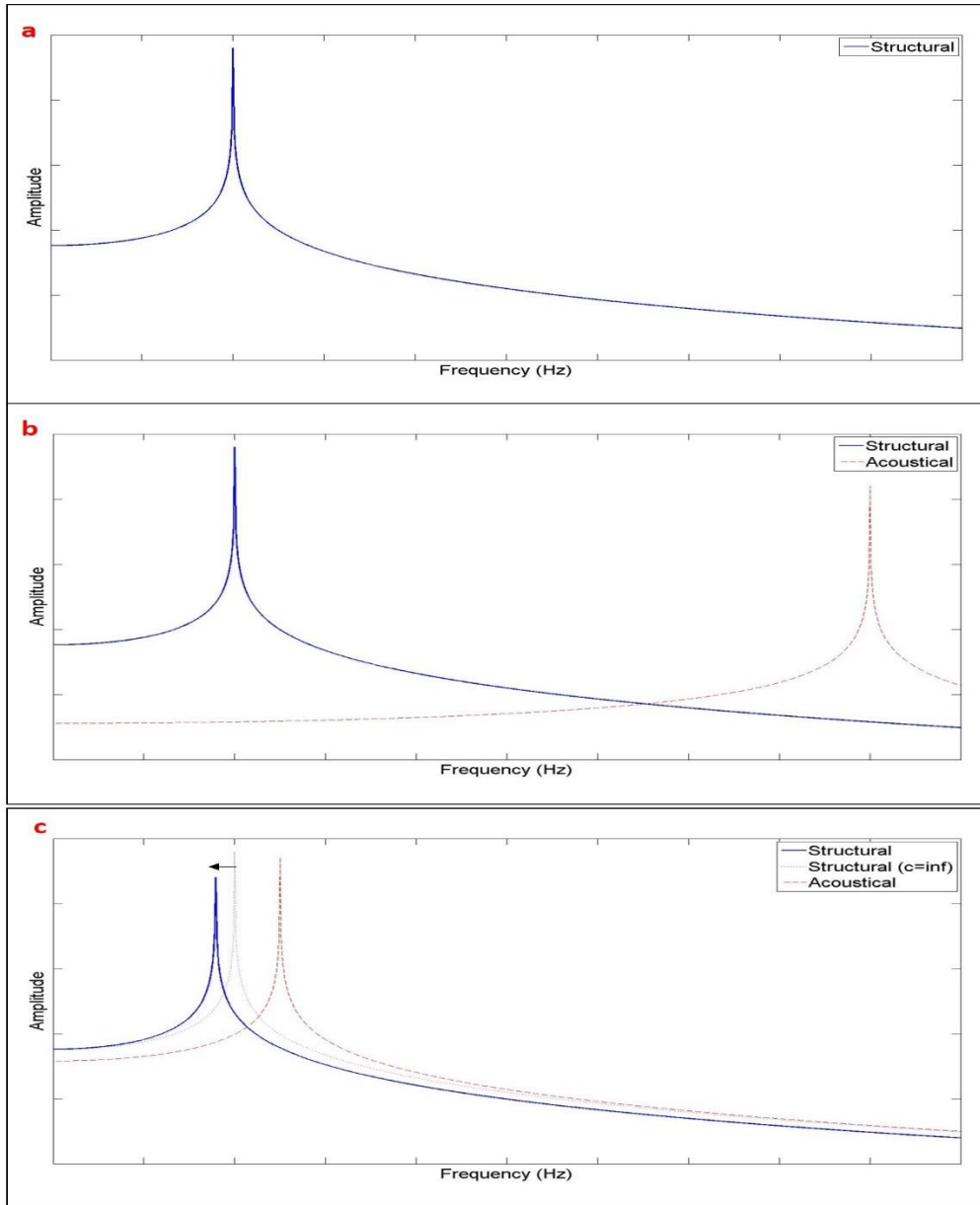


Figure 1. Influence of the speed of sound c on the structural modes, considering ρ_0 as a constant value. a) Structural mode with $c=\infty$ b) Structural mode with no influence of the acoustical mode. c) Structural mode affected by the acoustical mode.

3 FEM model

FEM numerical models have been demonstrated in many works to correctly estimate the natural frequencies of submerged structures using acoustic elements for modelling the surrounding fluid (Escaler et al., 2017; Huang et al., 2013a; Liang et al., 2007; Liang and Wang, 2003; Rodriguez et al., 2012; Valentín et al., 2014). Furthermore, the acoustic natural frequencies of the fluid cavity can be also determined using this method (Graf et al., 2014). This numerical method has been used to obtain all the results presented in the present paper.

The FEM model used consists of an annular disk submerged in a closed fluid cavity. The main dimensions of the model are shown in Figure 2. In order to study the influence of all the geometrical parameters, as well as material characteristics and boundary conditions, several simulations were carried out. One base case was defined in order to change all the different parameters one by one. The dimensions of this base case were based on the ones studied experimentally by Valentín et al. (2014).

The geometrical parameters that have been studied in this paper are the disk diameter (D) and the disk thickness (h_D). The boundary conditions that have been changed in the fluid cavity are the upper fluid distance (H_{up}), the lower fluid distance (H_{down}) and the radial gap (G) (see Figure 2). Moreover, both disk and fluid material densities (ρ_D, ρ_f) were varied as well as the speed of sound of the fluid (c). Table 1 summarizes all the parameters changed by simulation and in which range they were studied.

Table 1. Parameters changed by simulation

Parameter	From	to	Base case
h_D/D	0.01	0.10	0.04
H_{up}/D	0.20	0.38	0.20
H_{down}/D	0.02	0.20	0.20
G/D	0.0007	0.014	0.0014
ρ_f/ρ_D	0.000127	1.0	0.127
c	0	Infinite	1430 m/s

The numerical model was solved using ANSYS v16.2 (Ansys®, 2013). To take into account the fluid effect on the disk-like structure, the nodes of the solid parts in contact with the fluid are defined as Fluid-Structure Interaction (FSI) interface. This type of simulation assumes that the fluid is inviscid, irrotational, compressible and without mean flow. The disk is fixed in axial and radial directions by its interior diameter. Hexahedral mesh was selected to perform the simulations, using SOLID185 and FLUID30 elements type for the solid and fluid respectively. A mesh sensitivity study was performed in order to obtain the optimal mesh. This optimal mesh resulted to have approximately 38000 elements and it had less than 1% error with respect to the densest mesh tested. Simulations were conducted on an Intel® i7™ CPU at 2.67 GHz using a parallelized solver for 6 computational cores, and computation times ranged from 10 min to 15 min.

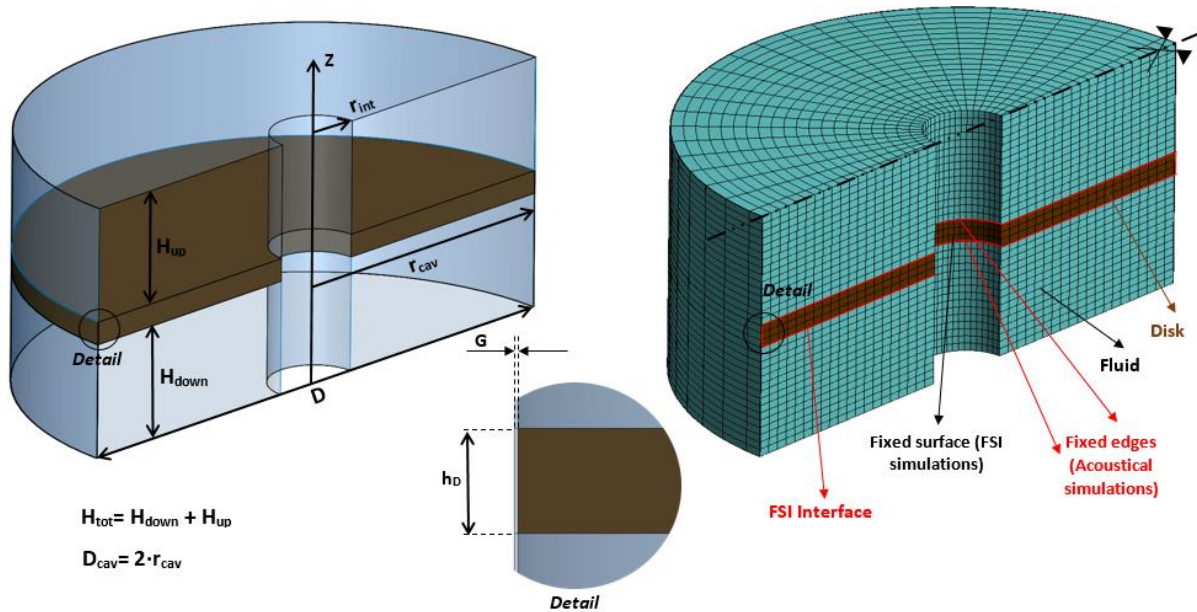


Figure 2. Detail of the mesh and the boundary conditions.

To analyse separately the influence of the added mass effect of the fluid and the influence of the acoustic part on the natural frequencies of the disk, three types of simulations were performed. First type of simulations were done with speed of sound infinite, flexible disk and varying geometrical (position and size of the disk and cavity) and material parameters (density of the disk and of the fluid). In this case the structural natural frequencies of the submerged and confined disk can be determined without any influence

of the acoustic natural frequencies of the cavity, as one can see in Figure 1a . Therefore, in this situation only the added mass effect considered in previous studies affects the natural frequencies of the disk.

Second type of simulations were done with variable speed of sound and totally rigid disk and walls. Size, dimensions and gaps of the fluid cavity were varied for this type of simulations. Therefore, the focus of these simulations is to determine the natural frequencies and mode shapes of the acoustical cavity without any influence of the structural part. Figure 1b represents this situation.

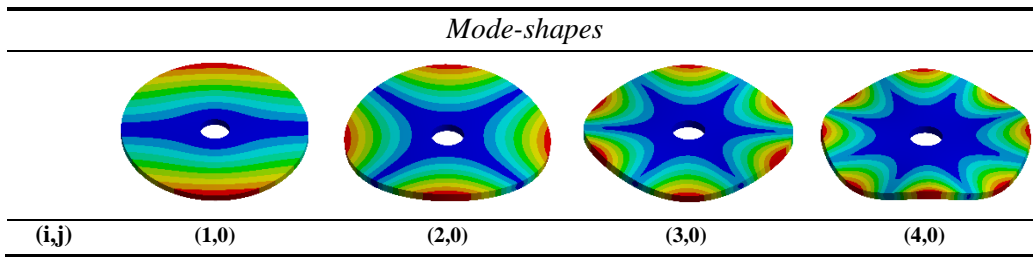
Finally, in order to study the natural frequencies of the submerged and confined disk affected by both the fluid added mass and the dynamic behaviour of the acoustic cavity (see Figure 1c), coupled simulations considering both fluid and structure were performed. The results were normalized to be used with different kind of geometrical dimensions and material characteristics.

4 Results and discussions

4.1 Structural natural frequencies and mode shapes of the disk.

The mode-shapes of a disk are defined by its number of nodal diameters (i) and nodal circles (j), (i,j) (see Table 2), (Blevins, 2001; Valentín et al., 2014).

Table 2. Mode-shapes of the disk.



The values of the natural frequencies of those mode-shapes in air can be easily obtained using reference (Blevins, 2001) and also with numerical simulations (Valentín et al., 2014). These natural frequencies depend basically on the geometry and material of the disk (diameter, thickness, density, Young modulus and Poisson's ratio).

For the base case ($h_D/D = 0.04$), the differences between the structural natural frequencies calculated by simulation using the FEM model and by the ones obtained theoretically in Blevins (2001) are listed in Table 3.

Table 3. Structural natural frequencies in air. Difference between simulation and theory.

Mode-shape (i,j)	δ (%)
(1,0)	-1.93
(2,0)	-3.58
(3,0)	-5.10
(4,0)	-5.63

Numerical results obtained with simulations are within deviations of 1.93% to 5.63% from the theoretical results. Therefore, numerical simulations are taken as a valid method to estimate natural frequencies of the structure in vacuum with good accuracy.

4.2 Added mass effect of the fluid

As predicted by many studies (see for example (Kwak, 1991; Lindholm et al., 1962; Meyerhoff, 1970)), submerging the structure into a heavy fluid (liquid) reduces its natural frequencies values due to the fluid

added mass. Fluid added mass depends on the geometrical dimensions of the fluid cavity, such as axial and radial gaps, and the structure and fluid densities. Nevertheless, the mode shapes of the submerged disk-like structure remains approximately the same than in the air (Amabili and Kwak, 1996). The effects of all these parameters have been studied in the present paper. It is interesting to point out that, as predicted by Coutu et al. (2012), Gauthier et al. (2017), Seeley et al. (2012) and Blevins (2001) there is an increase on the damping for a straight flow whilst fluid added mass is not significantly affected. Because of that, the values of structural natural frequencies remains practically equal for both the fluid still case and straight flow case. On the other hand, the case of rotational flow of a disk enclosed by a cylindrical cavity, is analytically, numerically and experimentally discussed by Presas et al. (2015b), Presas et al. (2015a) and Presas et al. (2016).

As explained in Section 3 with regard to the first type of simulations, to only take into account the added mass effect, the speed of sound of the fluid was considered as infinite (fluid incompressible) for this type of simulations. With respect to other studies (Askari et al., 2013; Valentín et al., 2014), the added mass factors obtained in these simulations are presented normalized for a wide range of geometrical and material characteristics of disks and fluid cavity (Figure 3, Figure A1-Figure A4 in Appendix A).

Figure 3 shows the results obtained for (2,0) mode-shape of the disk submerged in heavy fluid for the different parameters studied. Axial (H_{up}) and radial (G) gaps have been normalized using the disk diameter (D). In order to take the effect of the axial gap in only one side of the disk, H_{down} has been selected large enough to not affect the natural frequencies of the disk (increasing this value would not change the natural frequencies). The effect of considering a rigid wall in both axial sides of the disk, has been deeply discussed by (Presas et al., 2016). Generally, it is shown that the added mass effect is slightly increased when having this second gap.

Different ratios of disk thickness/disk diameter (h_D/D) have been studied. The fluid used for those simulations is water, with a density of 1000 kg/m^3 , whereas the disk material is stainless steel with a density of 7850 kg/m^3 ($\rho_f/\rho_D=0.127$). Introducing all the aforementioned parameters in this figure, the parameter δ can be obtained. Only modes with nodal diameters and no nodal circles have been considered in this study. In order to consider different G/D ratios, the correction factor λ has been introduced (Eq. (14)). This factor can be found in the table inside Figure 3 and Figure A1-Figure A4 in Appendix A.

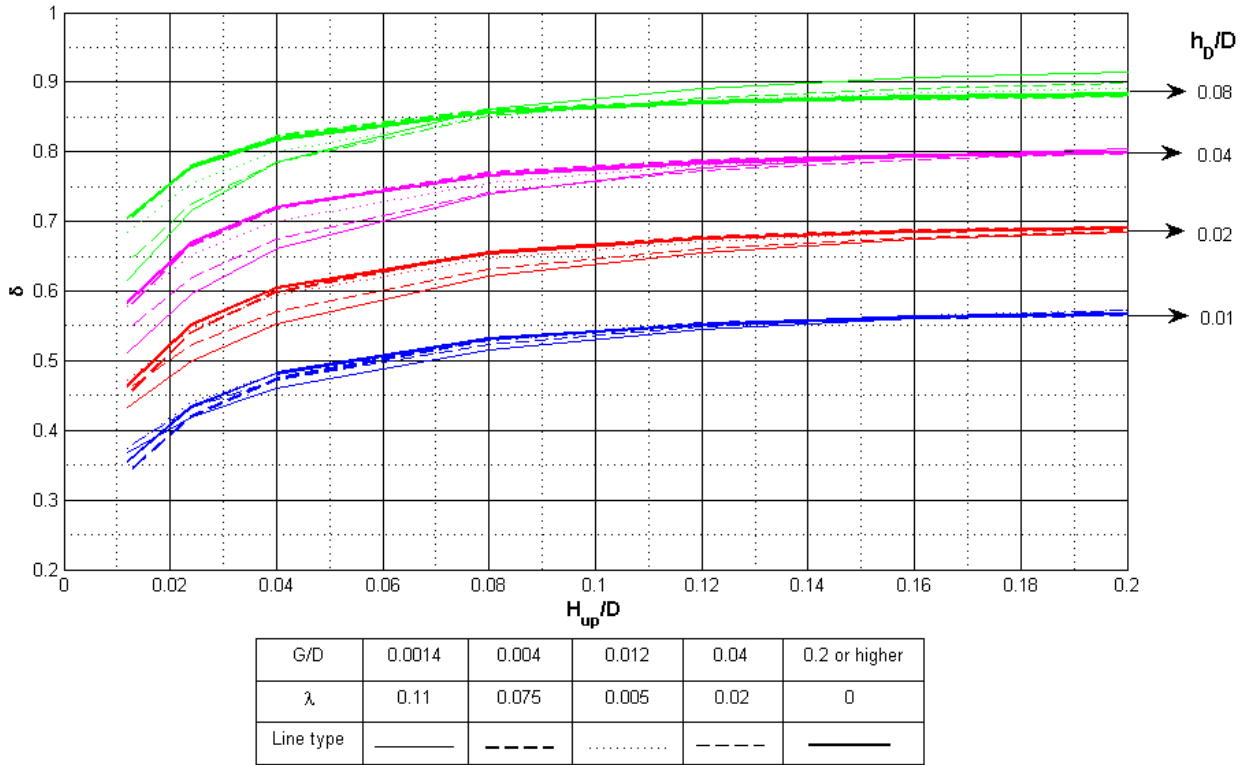


Figure 3. Fluid added mas factor. (2,0) mode-shape. Density ratio=0.127. $\Psi=1$.

Moreover, to consider different fluid-structure density ratios than water-stainless steel, several simulations were also carried out for $0.02 < \rho_f / \rho_D < 0.4$. The ρ_D was considered as a constant value and ρ_f was changed. Figure 4 shows the correction factor (ψ) (Eq. (14)) for different ρ_f / ρ_D ratios and different H_{up}/D for the mode (2,0) and constant h_D/D and G/D . The inverse procedure (changing ρ_D and taking ρ_f as constant) was also done and results obtained showed exactly the same values

The curves shown in Figure 4, can be approximated with a quadratic equation with a good accuracy for the represented range ($R^2=0.99$). The coefficients for this equation can be found in Appendix A (Table A1-Table A4) for different configurations of h_D/D and G/D and different mode-shapes.

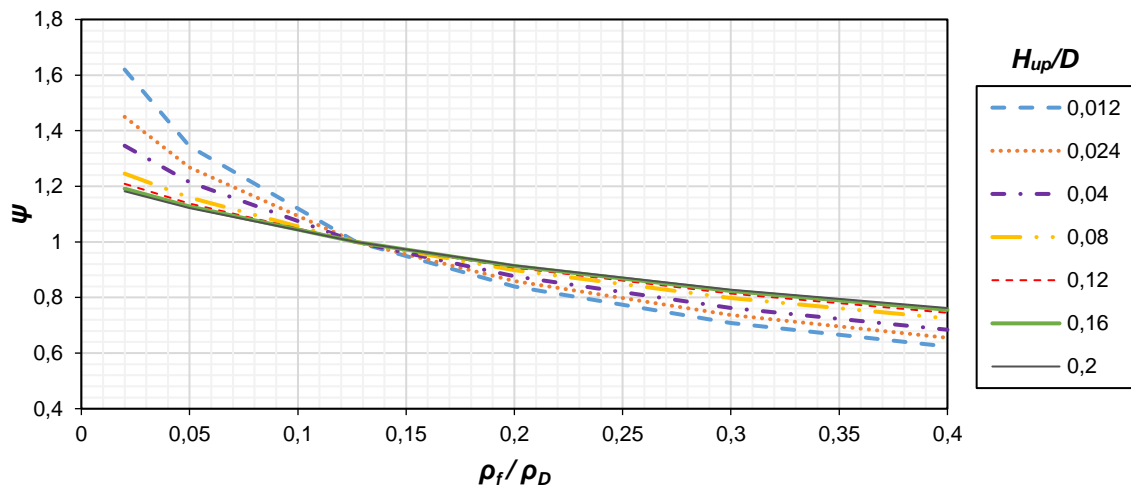


Figure 4. Influence of the density ratio on the added mass factor. (2,0) mode-shape. $h_D/D=0.08$; $G/D=0.0014$.

Finally, the natural frequency of the submerged disk with speed of sound infinite ($f_{f, c=\infty}$) is calculated using Eq. 14 introducing the parameters δ , λ and ψ , obtained in Figure A1-Figure A4 and Table A1-Table A4 (see Appendix A).

$$\frac{f_{f, c=\infty}}{f_{air}} = (\delta - \lambda) \cdot \psi \quad (14)$$

Figure 5 shows the added mass factor obtained using Eq. (14) for three geometrical configurations. These results are experimentally validated by Valentín et al. (2014) and Valentín et al. (2016) using the base case configuration and also by Presas et al. (2016), using a different disk and cavity dimensions. Numerical results presents a good agreement with the experimental ones. Then, the numerical simulations are validated to study fluid-structure interaction problems.

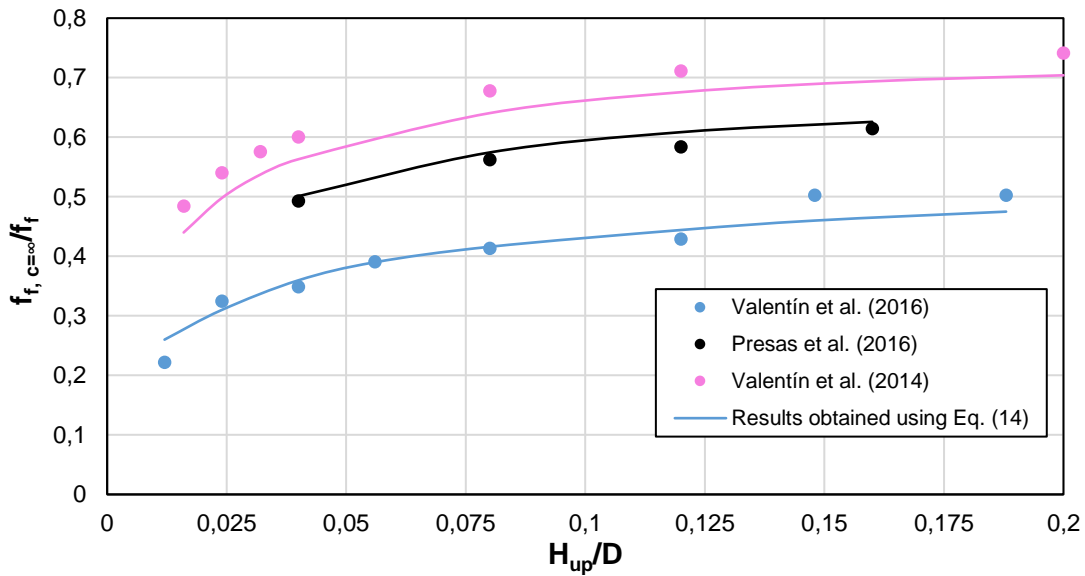


Figure 5. Added mass factor. Experimental results.

4.3 Acoustical natural frequencies of the fluid cavity

In order to know how acoustic natural frequencies can affect the structural natural frequencies of the disk, it is necessary to study first how acoustic mode-shapes are and which parameters can affect the acoustical natural frequencies. One of this parameters is the flowing velocity of the fluid which has been taken into account in some studies and results show that it acts as a damper of the acoustic mode (Brevart and Fuller, 1993; Tsuji et al., 2002). Therefore, the acoustic natural frequencies and acoustic mode shapes do not substantially change. For high velocity and low pressure flows where a significant cavitation volume can exist, the local speed of sound can be affected and therefore the acoustic natural frequencies can be drastically reduced as experimentally demonstrated by Shamsborhan et al. (2010) and Ruchonnet et al. (2012). This particular case is not discussed in the present paper.

For a cylindrical cavity with still fluid, the acoustical natural frequencies (f_{cav}) and its mode-shapes can be easily obtained using Eq. (15) extracted from Blevins (2001). The mode-shapes are formed again by nodal diameters (i), nodal circles (j), and number of cross sections (k) where the pressure is zero. The natural frequencies are linearly dependent on the speed of sound (c) and inversely proportional to the cavity radius (r_{cav}) and the cavity height (H_{tot}).

$$f_{cav,th} = \frac{c}{2 \cdot \pi} \left(\frac{\lambda_{ij}^2}{r_{cav}^2} + \frac{k^2 \pi^2}{H_{tot}^2} \right)^{1/2} \quad (15)$$

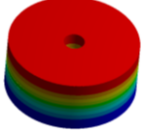


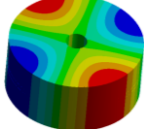
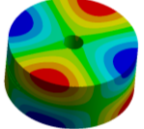
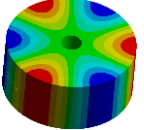
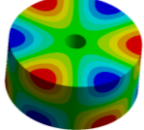
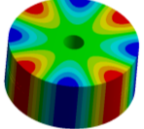
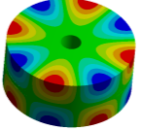
λ_{ij} is a parameter that depends on the mode-shape and it is given in Table 4. For this study only modes with nodal diameters have been considered, hence $j=0$.

Table 4. Parameter λ_{ij} . (Blevins, 2001).

Mode-shape (i,j)	λ_{ij}
(0,0)	0
(1,0)	1.8412
(2,0)	3.0542
(3,0)	4.2012
(4,0)	5.3176

These values have to be considered to calculate natural frequencies of a cylindrical cavity without any structure inside. Nevertheless, in the present case of study, the cavity contains a disk (Figure 2). To see which is the difference between considering or not the disk inside the cylindrical cavity for its acoustic natural frequencies, the second type of numerical simulations (see Section 3) with and without disk inside the fluid cavity were carried out for the dimensions of the base case. Results showed (see Table 5) that for the modes without any cross section ($k=0$), there is practically no difference, but for $k>0$ modes, this consideration is important. Therefore, Eq. (15) is only valid for the mode-shapes of the acoustical cavity with $k=0$ when a disk is submerged inside. For this case, the agreement between theory (Eq. (15)) and simulation is very good. In order to simplify nomenclature, modes with $k=0$ are henceforth named as global modes and modes with $k=1$ are named as **modes with cross section**.

Table 5. Acoustic natural frequencies and mode-shapes of the cavity. Comparison between theory and simulation using the base case configuration.

i	Mode-shape picture		Δ_{sim-th} (%)		$\Delta_{no\ disk-disk}$ (%)	
	k		k		k	
	0	1	0	1	0	1
0	-		-	0.00	-	-84.82
1			-5.21	-1.07	-0.02	-53.38
2			-0.54	-0.23	-0.02	-33.45
3			-0.16	-0.17	-0.07	-22.62
4			-0.28	-0.19	-0.03	-16.07

To evaluate the influence of the different geometrical parameters mentioned before (see Table 1) on the acoustic natural frequencies of the fluid cavity, the second type of simulations were performed again but changing these parameters. Results are shown in the following paragraphs.

4.3.1 Influence of the total height and axial gap.

Firstly, the length of the cavity (H_{tot}) has been changed maintaining the same distance above and below the disk ($H_{up} = H_{down}$) and then, several unsymmetrical configurations ($H_{up} \neq H_{down}$) remaining H_{tot} constant have been studied in order to understand how the acoustical natural frequencies of the fluid cavity are affected. Results are presented in a normalized way for a certain value of c .

Figure 6 shows the results obtained by changing H_{tot} , where global mode-shapes (a) and **modes with cross section** (b) are illustrated separately. The fluid depth (H_{tot}) is normalized against the diameter of the disk. The acoustic natural frequencies of the cavity, f_{cav} , are normalized against the acoustic natural frequencies obtained in the base case (Table 1 ($f_{cav,base}$)).

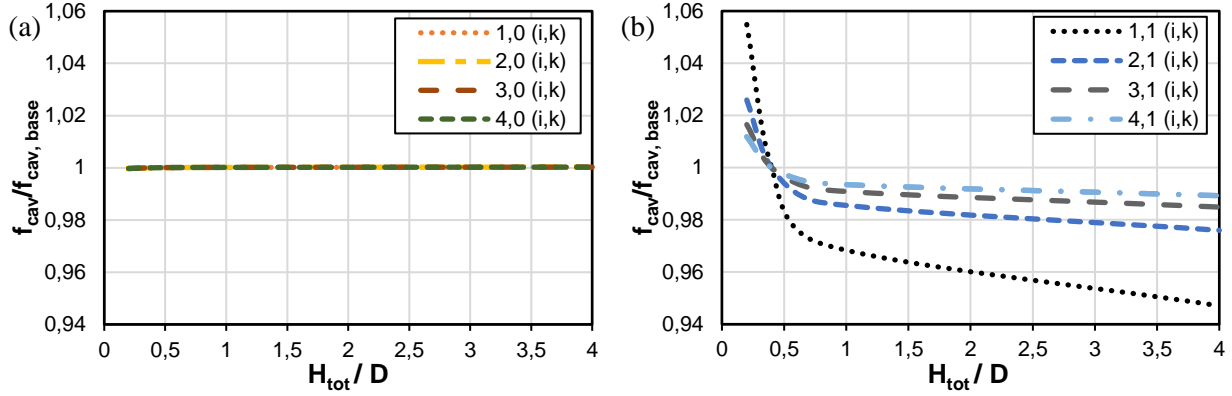


Figure 6. Total height. (a) Influence on the global modes, $k=0$. (b) Influence on the **modes with cross section**, $k=1$.

It is shown that varying H_{tot} , the acoustic frequency for the global modes remains practically constant (Figure 6a). However, for the **modes with cross section** (Figure 6b) the acoustic natural frequency value tends to decrease when increasing H_{tot} . These results (with disk inside the cavity) perfectly agree the theoretical results obtained with Eq. (15).

The effect of varying H_{up} along the Z coordinate is illustrated in Figure 7. Acoustic natural frequencies for global modes ($k=0$) are not affected when H_{up} decrease. However, in the **modes with cross section**, the axial gap has a greater effect on the (1,1) mode-shape for a $H_{up}/D > 0.35$ than on the higher ones ((2,1), (3,1), (4,1)). Therefore, the position of the disk is only important **for modes with cross section** ($k=1$) but not for the global modes ($k=0$).

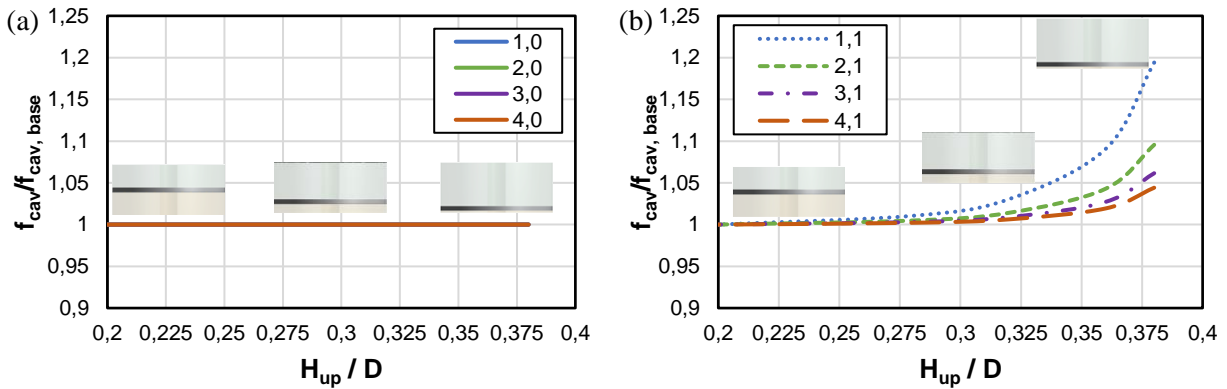


Figure 7. Influence of the axial gap on the acoustic natural frequencies. (a) Global modes. (b) **Modes with cross section**, $k=1$.

4.3.2 Influence of the radial gap

Regarding the radial gap, acoustic natural frequencies were studied for different values of G . The simulations were carried out for $7 \cdot 10^{-4} < G/D < 1.4 \cdot 10^{-2}$. Figure 8 shows the influence on the acoustic natural frequencies when G is changed. Global modes are slightly affected by the increment of G , (a reduction of 3% on the frequencies for a $G/D = 1.4 \cdot 10^{-2}$ have been found). The influence of G on the acoustic natural frequencies is higher for **modes with cross section** (Figure 8b). (1,0) mode-shape show higher differences than the higher ones ((2,0)-(4,0)) for a big radial gap ($G/D = 1.4 \cdot 10^{-2}$).

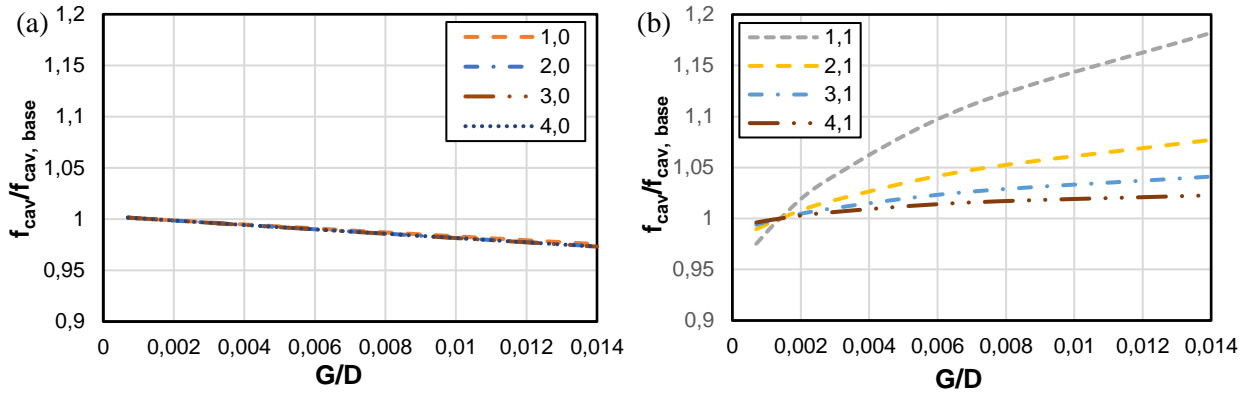


Figure 8. Influence of the radial gap on the acoustic frequencies. (a) Global modes. (b) Modes with cross section.

4.3.3 Influence of the cavity diameter

The variations of the acoustic natural frequencies by changing D_{cav} and maintaining the same radial gap (G) are seen in Figure 9. In the x-axis, D_{cav} have been normalized using the D_{cav} of the base case. In this case, it is appreciated that the importance of D_{cav} is high on the global mode-shapes as well as the modes with cross section, showing an increment on the acoustic natural frequencies between 75% and 200% for a $D_{cav}/D_{cav, base} < 0.5$; i.e. the higher the diameter of the disk is, the lower the acoustic natural frequencies are. This conclusion can be obtained also analysing Eq. (15).

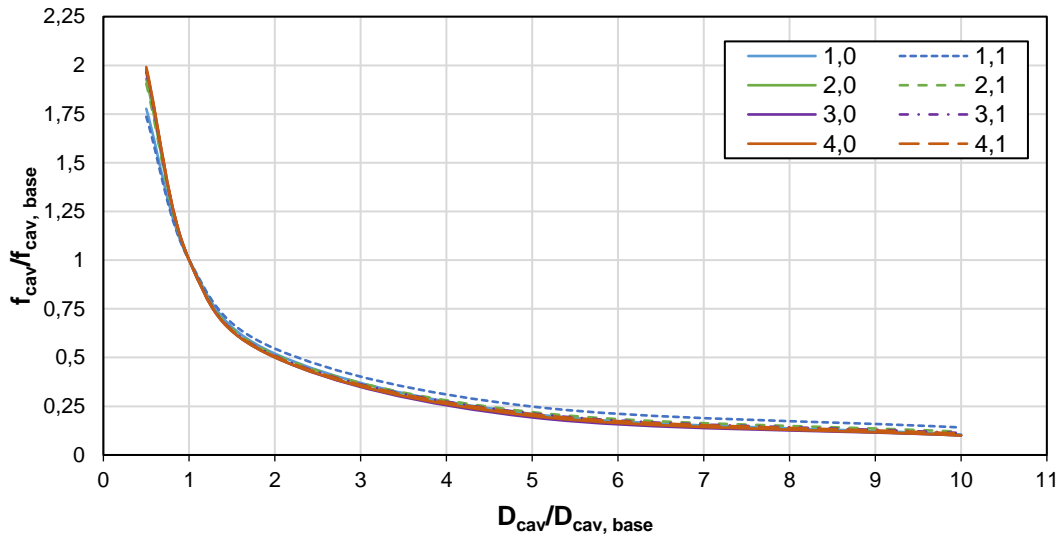


Figure 9. Influence of the diameter of the disk on acoustic natural frequencies.

Geometrical factors that can affect the acoustic natural frequencies of the cavity have been analysed. Modes with cross section are affected by the axial and radial gaps, as well as by the diameter of the cavity. The diameter of the cavity is the only parameter which affect considerably both mode-shapes, global modes and counter-phase modes. Global modes remain nearby constant when changing the rest of geometrical factors. This is an interesting conclusion because, no matter how the other dimensions are, the acoustic natural frequencies associated with the global mode-shapes can be simply obtained applying Eq. (15).

4.4 Coupled simulation

In this section the influence of the acoustic natural frequencies on the structural natural frequencies of the disk submerged in a fluid cavity is evaluated. Several coupled simulations (Third type, see Section 3) were carried out varying the speed of sound for $0.035 < c/c_0 < 1$ for the base case dimensional configurations. The fluid used for those simulations is water, with a density of 1000 kg/m^3 and c_0 of 1430 m/s , whereas the disk material is stainless steel with a density of 7850 kg/m^3 ($\rho_f/\rho_D = 0.127$). c_0 is the highest value that the speed of sound can have for a certain fluid (Yebra et al., 2017) at atmospheric pressure, 25°C and without the influence of any boundary condition.

The influence of the acoustical frequencies on the structural natural frequencies is shown in Figure 10. The acoustic natural frequencies of global mode-shapes of the fluid cavity, are plotted as solid lines. The y-axis represents natural frequency dimensionless using the disk diameter (D) and c_0 . In that way, the acoustical mode-shapes can be represented by just one line independently on the diameter.

The structural natural frequencies of the disk obtained for $c = \infty$ are plotted in dotted lines and they indicate the natural frequency of the disk without the influence of any acoustic natural frequencies of the cavity. These are the natural frequencies that can be obtained considering only the added mass effect, which has been deeply discussed in previous studies ((Amabili and Kwak, 1996; Kubota and Suzuki, 1984; Presas et al., 2016; Valentín et al., 2014) and that has been presented in this paper in a summarized way in Section 4.2 and Appendix A.

Finally the structural natural frequencies for different values of c are represented in dashed lines. These remain in the same value than with $c = \infty$ when they are far away from the acoustic natural frequencies lines. However, they start to decrease when they are near those lines. As it is explained on Section 2, by reducing the speed of sound, the fluid mass (M_f) becomes more significant on the fluid added mass term and therefore the natural frequencies of the disk starts to decrease. If the speed of sound is small enough, there is a point where the structural natural frequencies of the disk and the acoustic natural frequencies of the cavity have the same value. At this point, the fluid mass dominates over the disk mass, as explained in Section 2.

It is important to notice that the structural mode-shapes with no nodal circles are only affected by the acoustic mode-shape with the same number of nodal diameters also without nodal circles.

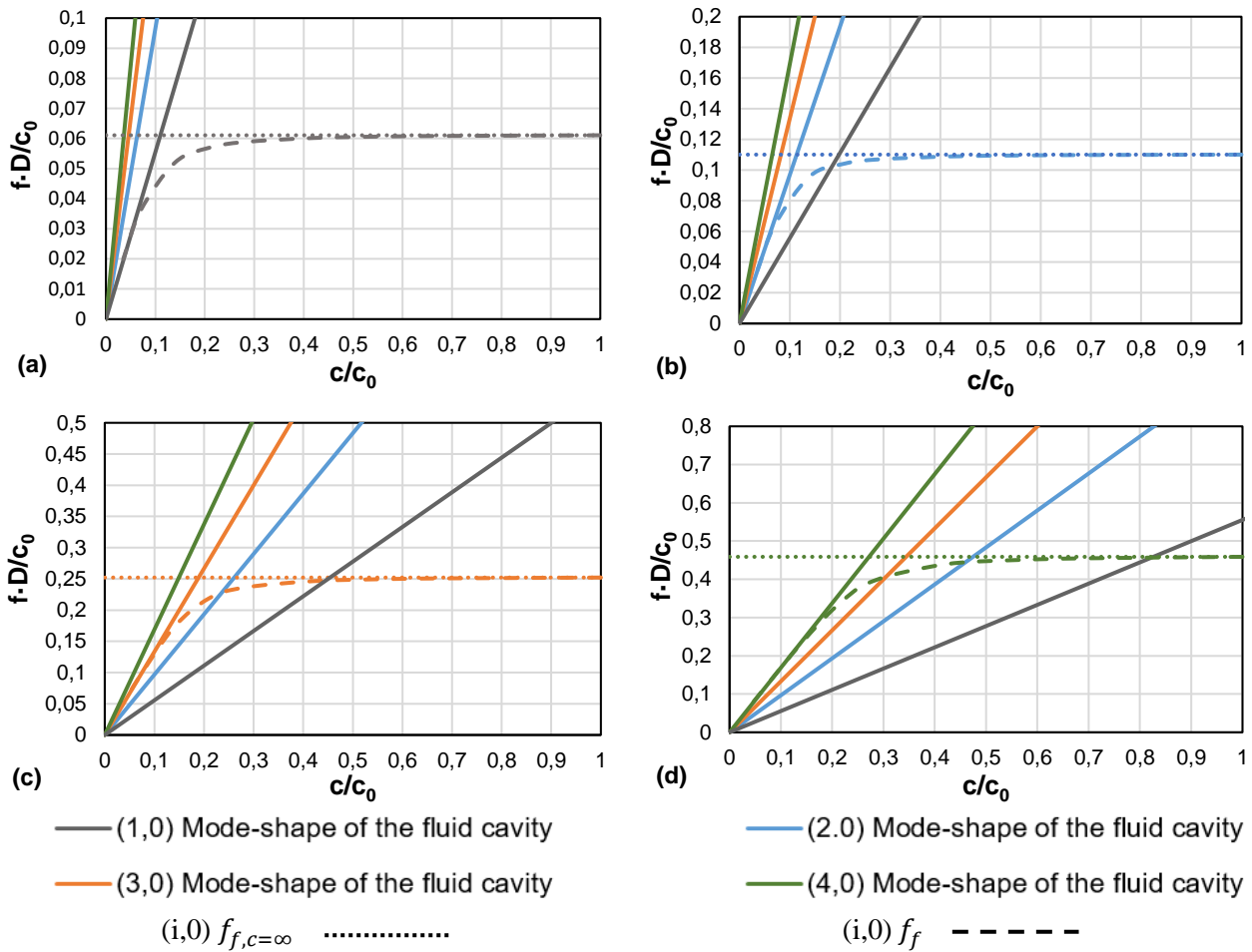


Figure 10. Coupled simulation. Acoustic and structural mode-shape. (1,0)(a). (2,0)(b). (3,0)(c). (4,0)(d)

With these results, it is demonstrated that depending on the mode-shape studied, always exist a speed of sound on which the structural natural frequency could be highly affected by the acoustic frequency of the cavity. To know for any kind of disk when (for which ratio c/c_0) its structural natural frequencies will be affected by the acoustic natural frequencies of the fluid cavity, the intersection point between the acoustic natural frequency line and the natural frequency line obtained with $c = \infty$ has to be analysed. This point can be obtained with more precision by using Figure A5 (see Appendix A) for any kind of disk.

Depending on the ratio c/c_0 obtained and the mode-shape, one can determine if the affectation of the structural natural frequency could be important on a real situation or even if it is already affected. An example case where the structural natural frequencies should not be affected by the acoustical cavity is shown in Figure 11. The $f_{f,c=\infty}$ of each global mode-shape of the base case are plotted as dotted lines. The cut point between the $f_{f,c=\infty}$ (i,0) line and the acoustic natural frequency (i,0) line has been highlighted. As one can see, the affectation on the structural natural frequency for each mode-shape occurs for $0.1 < c/c_0 < 0.3$ depending on the mode-shape. Actually, this is a non-very realistic situation because the speed of sound for this case should be very low in order that the acoustic natural frequencies affect the structural natural frequencies of the disk.

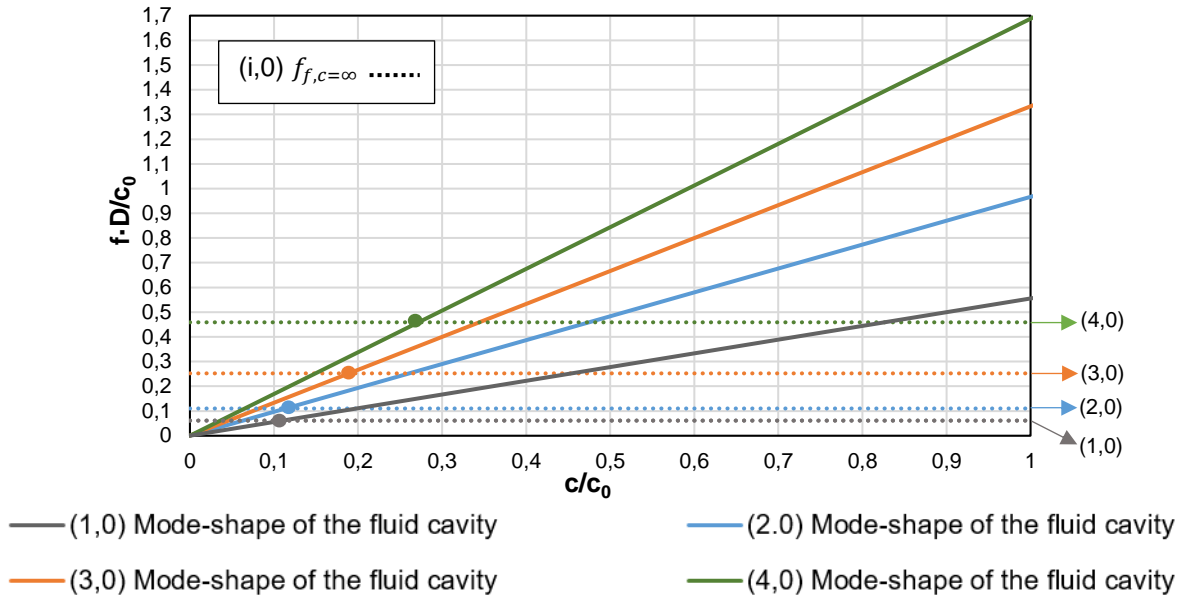


Figure 11. Base case. No affection for a real ratio c/c_0 .

However, for a certain geometrical configuration of the disk ($h_D/D= 0.12$ and $G/D= 0.012$ and $H_{up}/D =0.08$), this affection is found at a more realistic speed of sound value. Figure 12a shows the affection on the structural natural frequencies (dashed line) for $0.7 < c/c_0 < 0.8$ depending on the mode-shape. Both (1,0) and (2,0) modes are affected in this situation. However, (3,0) and (4,0) lines found for $c = \infty$ do not cross the acoustic natural frequencies lines before $c/c_0 < 1$ (dotted line of (4,0) is over the upper limit of the range and therefore does not cross before $c/c_0 < 1$). This means that those structural mode-shapes are already affected by the acoustical mode-shapes for the maximum value of speed of sound of the studied fluid (Yebra et al., 2017). This situation is representative of certain large hydraulic turbines.

A different geometrical configuration ($h_D/D= 0.13$ and $G/D= 0.012$ and $H_{up}/D =0.08$) has been also considered. Results are shown in Figure 12b. In this situation, the $f_{f,c=\infty}$ for each (i,0) mode-shape is higher than the acoustic natural frequency (with the same number of nodal diameters) at $c/c_0=1$. Then, the structural natural frequency of each mode-shape of the disk is affected by the acoustic natural frequencies for all c/c_0 . That means that in this case the value of the speed of sound has to be known and taken into account in order to accurately calculate the natural frequencies of the disk.

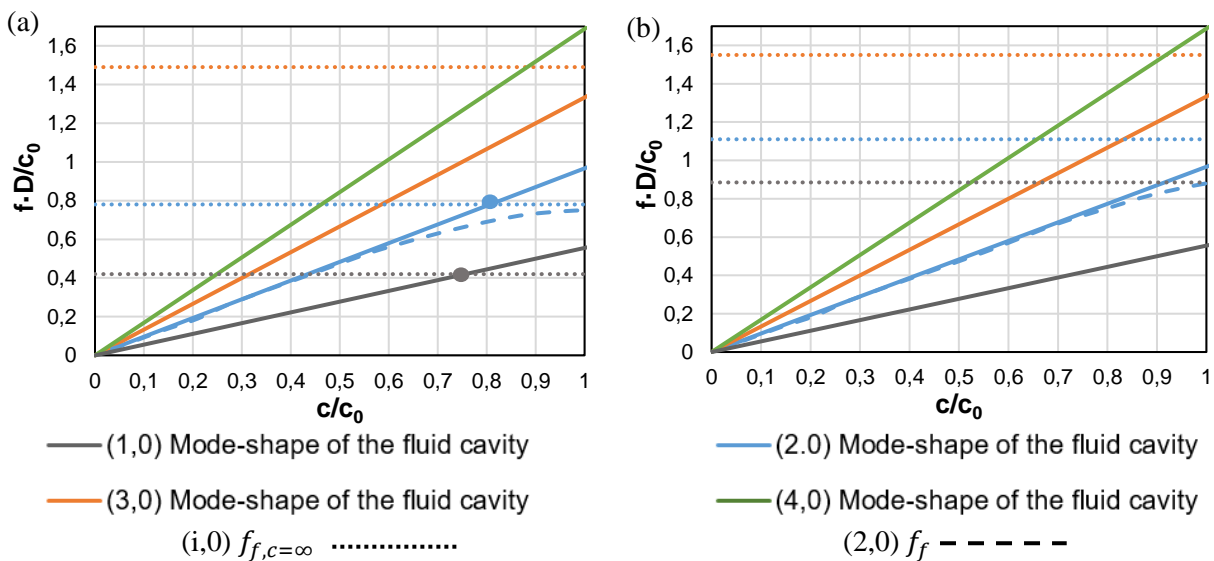


Figure 12. Intersection points for two geometrical configurations. (a) Real ratio c/c_0 . (b) Affection for all ratio c/c_0 .

4.4.1 Influence of the density of the fluid.

The simulations of the previous sections were conducted taking into account the ratio $\rho_f/\rho_D = 0.127$. This ratio represents a common engineering application, where the steel and water are the typical materials. In this section, the influence of different ratios ρ_f/ρ_D on the dynamic behaviour of the submerged disk is evaluated. Because of that, numerical simulations were carried out for $1.27 \cdot 10^{-4} \leq \rho_f/\rho_D \leq 1$, varying ρ_f and maintaining ρ_D constant. The geometrical parameters of the base case were used. Results obtained are shown in Figure 13 for the (2,0) structural mode shape. In this figure, $f_{f,c=\infty}$ for every case is plotted in dotted line, f_f is plotted in solid line and the (2,0) acoustic mode shape is the single dashed line (it is the same for all configurations since the acoustic natural frequency does not depend on the fluid density (Eq. (15))). The cut point between the $f_{f,c=\infty}$ line and the acoustic natural frequency line has been highlighted in this graph. The difference in percentage between this point and the actual value of the structural natural frequency (f_f) has been named as φ . It can be observed that the higher is the ratio ρ_f/ρ_D , the higher is φ . This means that for higher ratios ρ_f/ρ_D , the influence of the acoustic natural frequency on the structural natural frequency is higher.

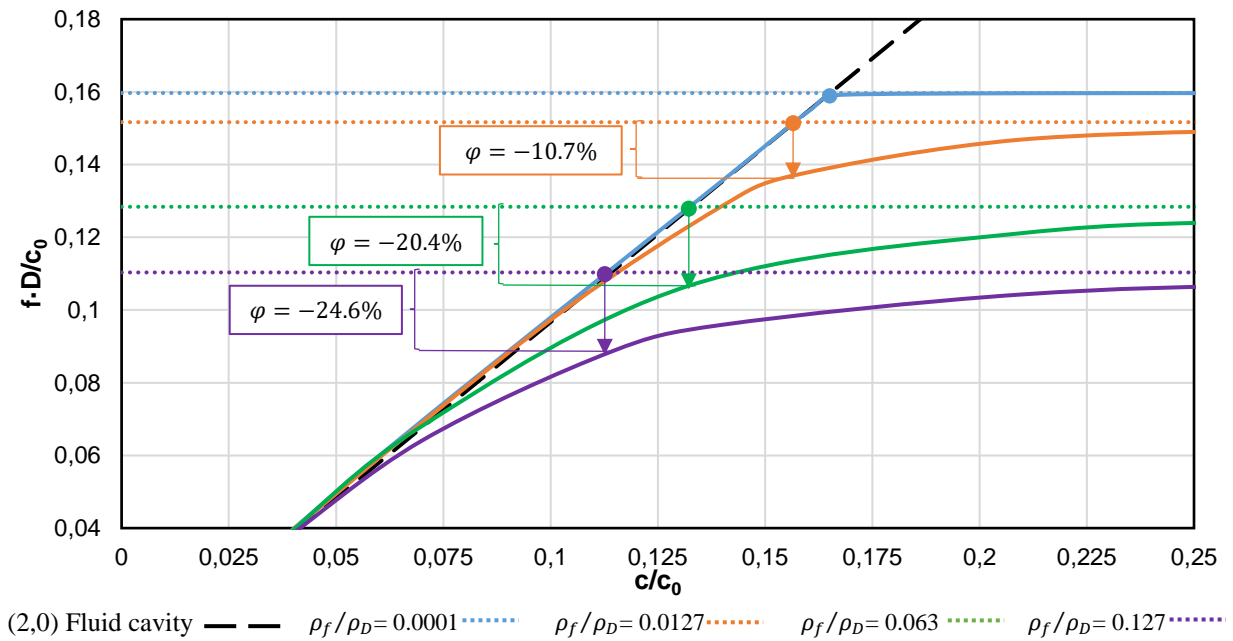


Figure 13. Results of the influence of the density ratio on the structural mode-shape. (2,0)

To evaluate the influence of the ratio ρ_f/ρ_s for the (1,0), (2,0), (3,0) and (4,0) mode-shapes, the same procedure was repeated. Results are shown in Figure 14. In this figure, φ is plotted for different ratios ρ_f/ρ_D and mode-shapes. It is observed that the biggest changes in φ are in the zone of the smallest ρ_f/ρ_D ratios (from 0 to 0.2). For ratios ρ_f/ρ_D higher than 0.2, φ is still decreasing but slowly. As commented before, these results were obtained changing ρ_f and maintaining ρ_D constant. However, to ensure the use of this graphic for all kind of materials, the inverse procedure (changing ρ_D and maintaining ρ_f) was done and results obtained showed exactly the same values than plotted in Figure 14 for the same ratios (ρ_f/ρ_D). With this information and the cut point obtained from Figure A5, one can obtain the influence of the acoustic natural frequency on the structural natural frequency for all kind of disks with different geometrical and material characteristics submerged and confined in different kind of fluids.

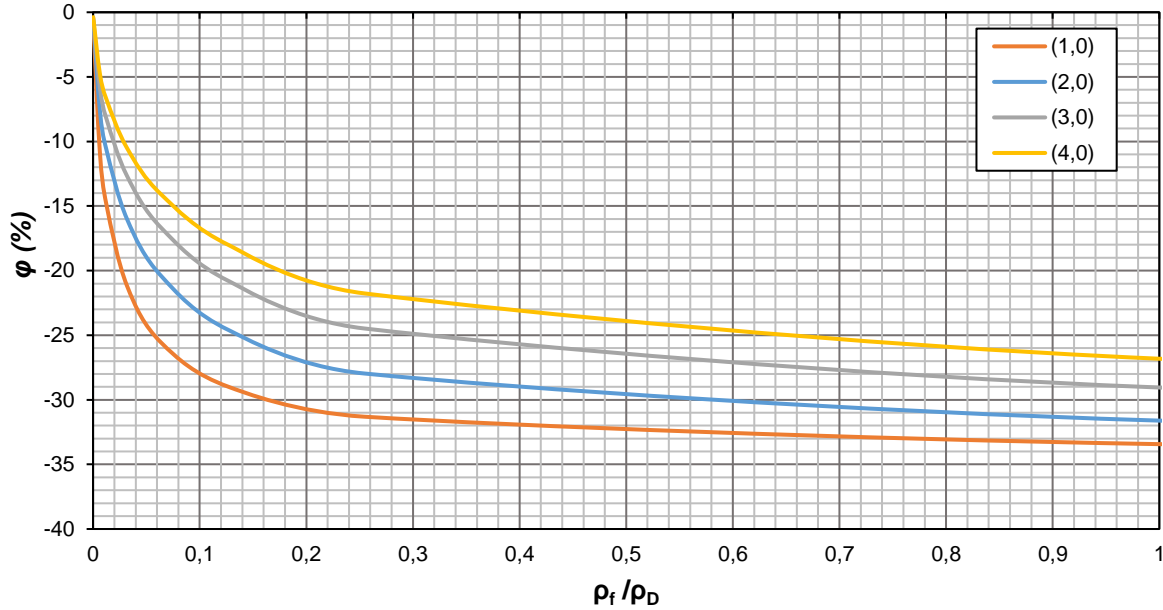


Figure 14. Density reduction ratio for a generic confined disk-like structure.

5 Conclusions

In this paper, the natural frequencies of submerged and confined disks have been studied when they are close to the acoustical natural frequencies of the surrounding fluid cavity. For this purpose, first, the natural frequencies of submerged disks have been studied considering that the acoustic natural frequencies of the surrounding fluid cavity are much higher than the disk natural frequencies. For this case, the most important geometrical and material parameters that can affect them have been analysed. Then, the parameters that affect the acoustical natural frequencies of the fluid cavity have been identified. Finally, the case with acoustic natural frequencies close to the disk natural frequencies have been studied and discussed in detail.

Acoustical natural frequencies of a fluid cavity are mainly dependent on the cavity dimensions and the speed of sound. The influence of different geometrical parameters (height of the cavity, axial gap and radial gap to the disk, and diameter of the cavity) have been determined in this paper. Results showed that for global mode-shapes ($k=0$), the only geometrical parameter that mainly affect the natural frequency of the cavity is the diameter, **mode-shapes with cross section** ($k>0$) all the aforementioned parameters change the natural frequency value. Speed of sound linearly increase the value of all acoustical natural frequencies.

When the acoustical natural frequencies are much higher than the disk natural frequencies, only the added mass effect of the fluid affects the disk natural frequencies. This added mass depends on the geometrical characteristics of the disk and gaps to the proximity walls, as well as the material properties. With respect to other studies about added mass in submerged and confined disks, in this paper the results have been presented in a dimensionless way in order to be able to obtain the natural frequencies of the submerged disk for different diameter, thickness, axial gap, radial gap of the disk and different structure-fluid densities. Moreover, numerical results obtained have been compared with experimental results obtained in previous studies and they accurately agree.

The case with acoustic natural frequencies close to the disk natural frequencies has been analysed in detail for a wide range of geometrical and material conditions. Speed of sound have been varied in order to approach the acoustical natural frequency values to the disk natural frequencies. It has been demonstrated that for certain geometrical characteristics of disk and cavity, the structural natural frequencies can be affected considerably. For a common engineering application where stainless steel and water are the typical materials, structural natural frequencies could be reduced about 25% by the acoustic natural frequencies. It has been also demonstrated that the disk natural frequencies are only affected by the acoustical natural

frequencies associated to an acoustical mode-shape with the same number of nodal diameters than the structural mode-shape. If the number of nodal diameters of both acoustical and structural mode-shapes does not coincide, the natural frequencies are not affected.

All the necessary information to apply the results obtained in this investigation to a wide range of confined disks is given. As a first approach, one can determine if the natural frequencies of a certain disk will be affected by the acoustical natural frequencies of the surrounding fluid cavity using the results presented in this paper, without needing any numerical simulations.

Acknowledgments

The authors acknowledge the European Project HYPERBOLE “HYdropower plants PERformance and flexiBle Operation towards Lean integration of new renewable Energies”, FP7-ENERGY-2013-1 for the technical and economic support received for developing this work. The authors also wish to acknowledge Voith Hydro Holding GmbH & Co. KG for the technical support received for developing this work.

References

- Amabili, M., Kwak, M., 1996. Free vibrations of circular plates coupled with liquids: revising the Lamb problem. *Journal of Fluids and Structures* 10, 743-761.
- Ansys®, 2013. ANSYS Mechanical User's Guide 15.0, Canonsburg, USA.
- Askari, E., Jeong, K., Amabili, M., 2013. Hydroelastic vibration of circular plates immersed in a liquid filled container with free surface. *Journal of Sound and Vibration* 332, 3064-3085.
- Bauer, H.F., Eidel, W., 2007. Transverse vibration and stability of spinning circular plates of constant thickness and different boundary conditions. *Journal of Sound and Vibration* 300, 877-895.
- Blevins, R.D., 2001. *Formulas for Natural Frequency and Mode Shape*. Krieger Publishing Company.
- Brevart, B., Fuller, C., 1993. Effect of an internal flow on the distribution of vibrational energy in an infinite fluid-filled thin cylindrical elastic shell. *Journal of sound and Vibration* 167, 149-163.
- Campbell, W., 1924. Protection of steam turbine disk wheels from axial vibration. *Transactions of the ASME* 46, 31-160.
- Coutu, A., Seeley, C., Monette, C., Nennemann, B., Marmont, H., 2012. Damping measurements in flowing water, *IOP Conference Series: Earth and Environmental Science*. IOP Publishing, p. 062060.
- Dowling, A.P., Stow, S.R., 2003. Acoustic analysis of gas turbine combustors. *Journal of propulsion and power* 19, 751-764.
- Egusquiza, E., Valero, C., Huang, X., Jou, E., Guardo, A., Rodriguez, C., 2012. Failure investigation of a large pump-turbine runner. *Engineering Failure Analysis* 23, 27-34.
- Escaler, X., De La Torre, O., Goggins, J., 2017. Experimental and numerical analysis of directional added mass effects in partially liquid-filled horizontal pipes. *Journal of Fluids and Structures* 69, 252-264.
- Gauthier, J., Giroux, A., Etienne, S., Gosselin, F., 2017. A numerical method for the determination of flow-induced damping in hydroelectric turbines. *Journal of Fluids and Structures* 69, 341-354.
- Graf, T., Gisler, T., Sollberger, P., Schälli, O., 2014. *Acoustic Wave Propagation in Water Filled Buried Polyethylene Pipes*, Comsol Conference, Cambridge.
- Harrison, C., Tavernier, E., Vancauwenberghe, O., Donzier, E., Hsu, K., Goodwin, A.R., Marty, F., Mercier, B., 2007. On the response of a resonating plate in a liquid near a solid wall. *Sensors and Actuators A: Physical* 134, 414-426.
- Heo, J.W., Chung, J., 2004. Vibration analysis of a flexible rotating disk with angular misalignment. *Journal of Sound and Vibration* 274, 821-841.
- Huang, X., 2011. *Contribution to the Dynamic Response of Hydraulic Turbomachinery Components*.
- Huang, X., Egusquiza, E., Valero, C., Presas, A., 2013a. Dynamic behaviour of pump-turbine runner: From disk to prototype runner, *IOP Conference Series: Materials Science and Engineering*. IOP Publishing, p. 022036.

Huang, X., Valero, C., Egusquiza, E., Presas, A., Guardo, A., 2013b. Numerical and experimental analysis of the dynamic response of large submerged trash-racks. *Computers & Fluids* 71, 54-64.

Jourdain, G., Eriksson, L.-E., Kim, S.H., Sohn, C.H., 2013. Application of dynamic mode decomposition to acoustic-modes identification and damping in a 3-dimensional chamber with baffled injectors. *Journal of Sound and Vibration* 332, 4308-4323.

Kousen, K.A., 1999. Eigenmodes of ducted flows with radially-dependent axial and swirl velocity components.

Kubota, Y., Ohashi, H., 1991. A study of the natural frequencies of hydraulic pumps. *Proceedings of the 1st JSME/ASME Joint International Conference on Nuclear Engineering*, Tokyo, 589-593.

Kubota, Y., Suzuki, T., 1984. Added mass effect on disc vibrating in fluid. *Transactions of the Japan Society of Mechanical Engineers* 50, 243-248.

Kwak, M.K., 1991. Vibration of circular plates in contact with water. *Journal of Applied Mechanics* 5, 205-216.

Lamb, H., Southwell, R.V., 1921. The vibrations of a spinning disk. *Proceedings of the Royal Society of London* 99, 272-280.

Liang, Q., Rodriguez, C., Egusquiza, E., Escaler, X., Farhat, M., Avellan, F., 2007. Numerical simulation of fluid added mass effect on a francis turbine runner. *Computers & Fluids* 36, 1106-1118.

Liang, Q., Wang, Z., 2003. Strength and vibration analysis of a francis turbine. *Qinghua Daxue Xuebao/Journal of Tsinghua University(China)* 43, 1649-1652.

Lindholm, U.S., Kana, D.D., Chu, W.-H., Abramson, H.N., 1962. ELASTIC VIBRATION CHARACTERISTICS OF CANTILEVER PLATES IN WATER. DTIC Document.

Meyerhoff, W., 1970. Added masses of thin rectangular plates calculated from potential theory. *J. Ship Res* 14, 100-111.

Naik, T., Longmire, E.K., Mantell, S.C., 2003. Dynamic response of a cantilever in liquid near a solid wall. *Sensors and Actuators A: physical* 102, 240-254.

Nieter, J.J., Singh, R., 1982. Acoustic modal analysis experiment. *The Journal of the Acoustical Society of America* 72, 319-326.

Presas, A., Valentin, D., Egusquiza, E., Valero, C., Seidel, U., 2015a. Influence of the rotation on the natural frequencies of a submerged-confined disk in water. *Journal of Sound and Vibration* 337, 161-180.

Presas, A., Valentin, D., Egusquiza, E., Valero, C., Seidel, U., 2015b. On the detection of natural frequencies and mode shapes of submerged rotating disk-like structures from the casing. *Mechanical Systems and Signal Processing* 60, 547-570.

Presas, A., Valentin, D., Egusquiza, E., Valero, C., Seidel, U., 2016. Dynamic response of a rotating disk submerged and confined. Influence of the axial gap. *Journal of Fluids and Structures* 62, 332-349.

Presas, A., Valero, C., Huang, X., Egusquiza, E., Farhat, M., Avellan, F., 2012. Analysis of the dynamic response of pump-turbine runners-Part I: Experiment, *IOP Conference Series: Earth and Environmental Science*. IOP Publishing, p. 052015.

Rodriguez, C., Egusquiza, E., Escaler, X., Liang, Q., Avellan, F., 2006. Experimental investigation of added mass effects on a Francis turbine runner in still water. *Journal of Fluids and Structures* 22, 699-712.

Rodriguez, C.G., Flores, P., Pierart, F.G., Contzen, L.R., Egusquiza, E., 2012. Capability of structural-acoustical FSI numerical model to predict natural frequencies of submerged structures with nearby rigid surfaces. *Computers & Fluids* 64, 117-126.

Rossetto, G., Arruda, J., Huallpa, B., 2001. Experimental modal analysis of a cavity using a calibrated acoustic actuator, *PROCEEDINGS OF THE INTERNATIONAL SEMINAR ON MODAL ANALYSIS*. KU Leuven; 1998, pp. 1415-1422.

Ruchonnet, N., Alligné, S., Nicolet, C., Avellan, F., 2012. Cavitation influence on hydroacoustic resonance in pipe. *Journal of Fluids and Structures* 28, 180-193.

Scholl, D., Davis, C., Russ, S., Barash, T., 1998. The volume acoustic modes of spark-ignited internal combustion chambers. *SAE Technical Paper*.

Seeley, C., Coutu, A., Monette, C., Nennemann, B., Marmont, H., 2012. Characterization of hydrofoil damping due to fluid-structure interaction using piezocomposite actuators. *Smart Materials and Structures* 21, 035027.

Shamsborhan, H., Coutier-Delgosha, O., Caignaert, G., Nour, F.A., 2010. Experimental determination of the speed of sound in cavitating flows. *Experiments in Fluids* 49, 1359-1373.

Southwell, R.V., 1922. On the free transverse vibrations of a uniform circular disk clamped at its center and on the effects of rotation. *Proceedings of the Royal Society of London* 101, 133-153.

Tanaka, H., 2011. Vibration behavior and dynamic stress of runners of very high head reversible pump-turbines. *International Journal of Fluid Machinery and Systems* 4, 289-306.

Tsuji, T., Tsuchiya, T., Kagawa, Y., 2002. Finite element and boundary element modelling for the acoustic wave transmission in mean flow medium. *Journal of Sound and Vibration* 255, 849-866.

Valentín, D., Presas, A., Egusquiza, E., Valero, C., 2014. Experimental study on the added mass and damping of a disk submerged in a partially fluid-filled tank with small radial confinement. *Journal of Fluids and Structures* 50, 1-17.

Valentín, D., Presas, A., Egusquiza, E., Valero, C., Egusquiza, M., 2016. Experimental study of a vibrating disk submerged in a fluid-filled tank and confined with a non-rigid cover. *Journal of Vibration and Acoustics*.

Yebra, F., Troncoso, J., Romaní, L., 2017. Fully automatized apparatus for determining speed of sound for liquids in the temperature and pressure interval (283.15–343.15) K and (0.1–95) MPa. *The Journal of Chemical Thermodynamics* 104, 102-109.

Appendix A

A1 Fluid added mass. δ and λ factors.

A.1.1. (1,0) Mode-shape.

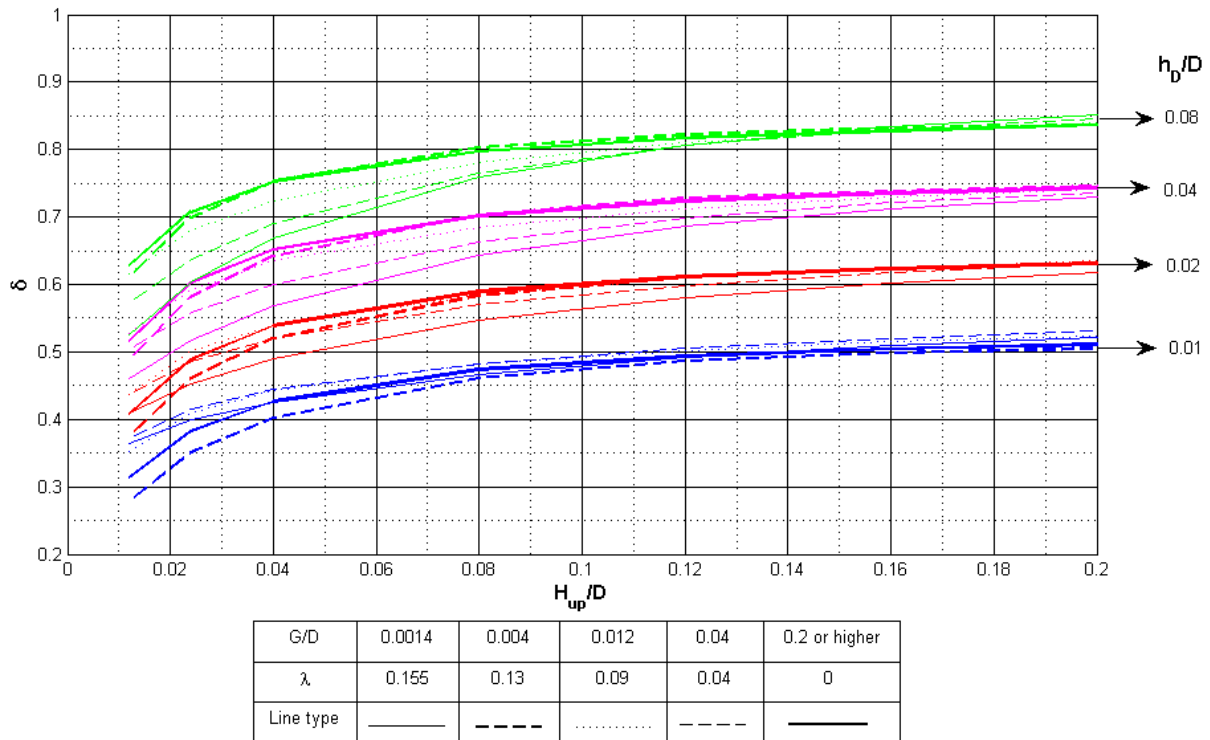


Figure A1. Added mass factor. (1,0) mode-shape

A.1.2. (2,0) Mode-shape

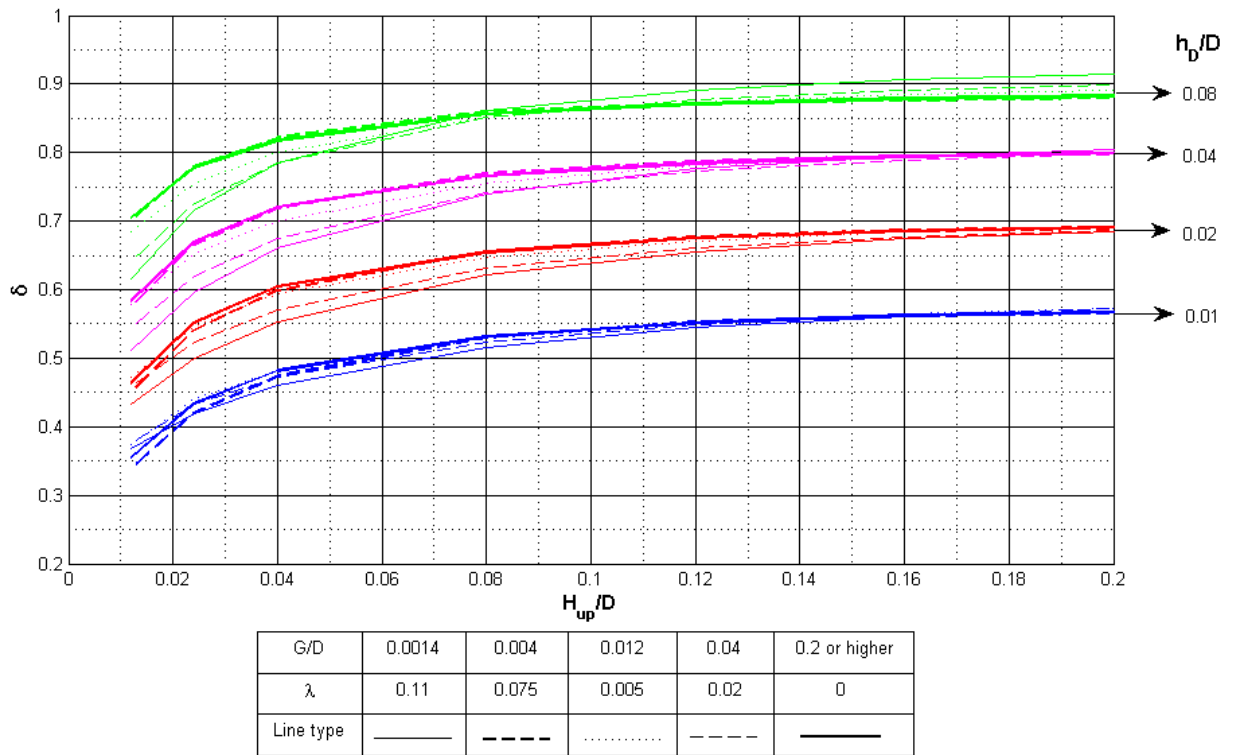


Figure A2. Added mass factor. (2,0) mode-shape.

A.1.3. (3,0) Mode-shape

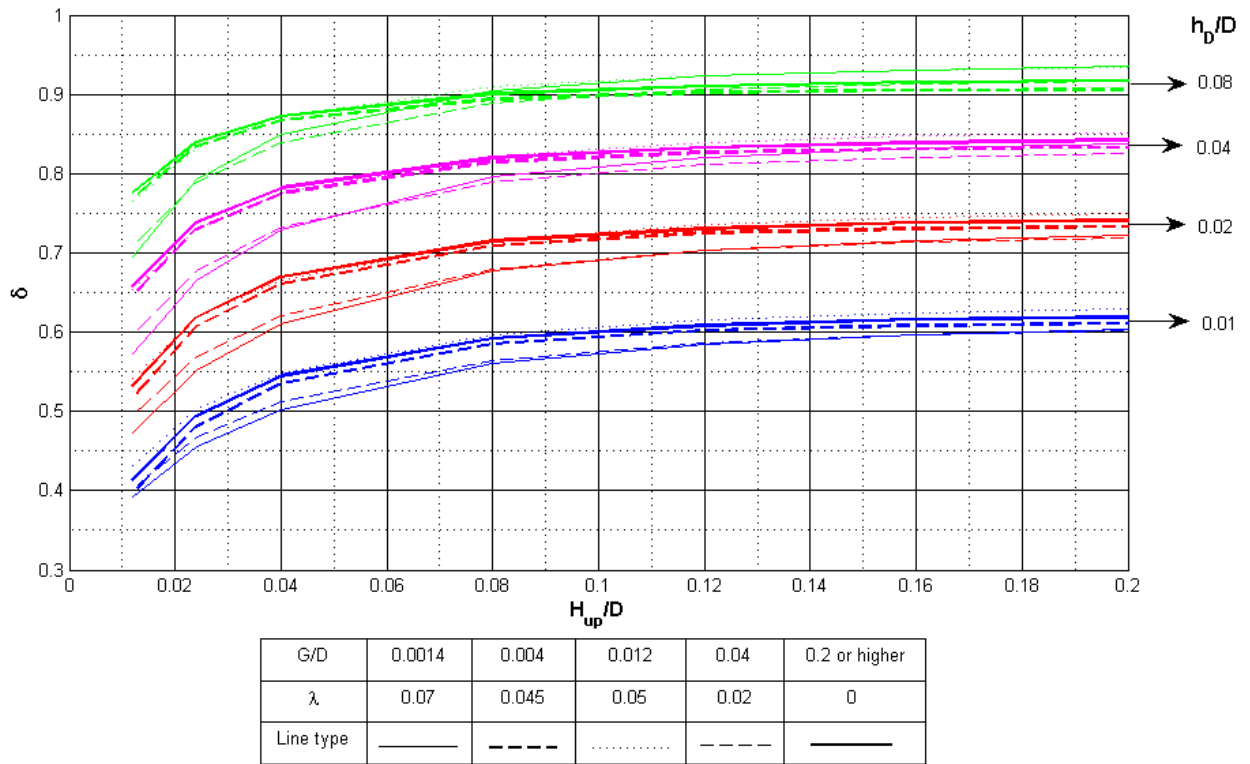


Figure A3. Added mass factor. (3,0) mode-shape.

A.1.4. (4,0) Mode-shape

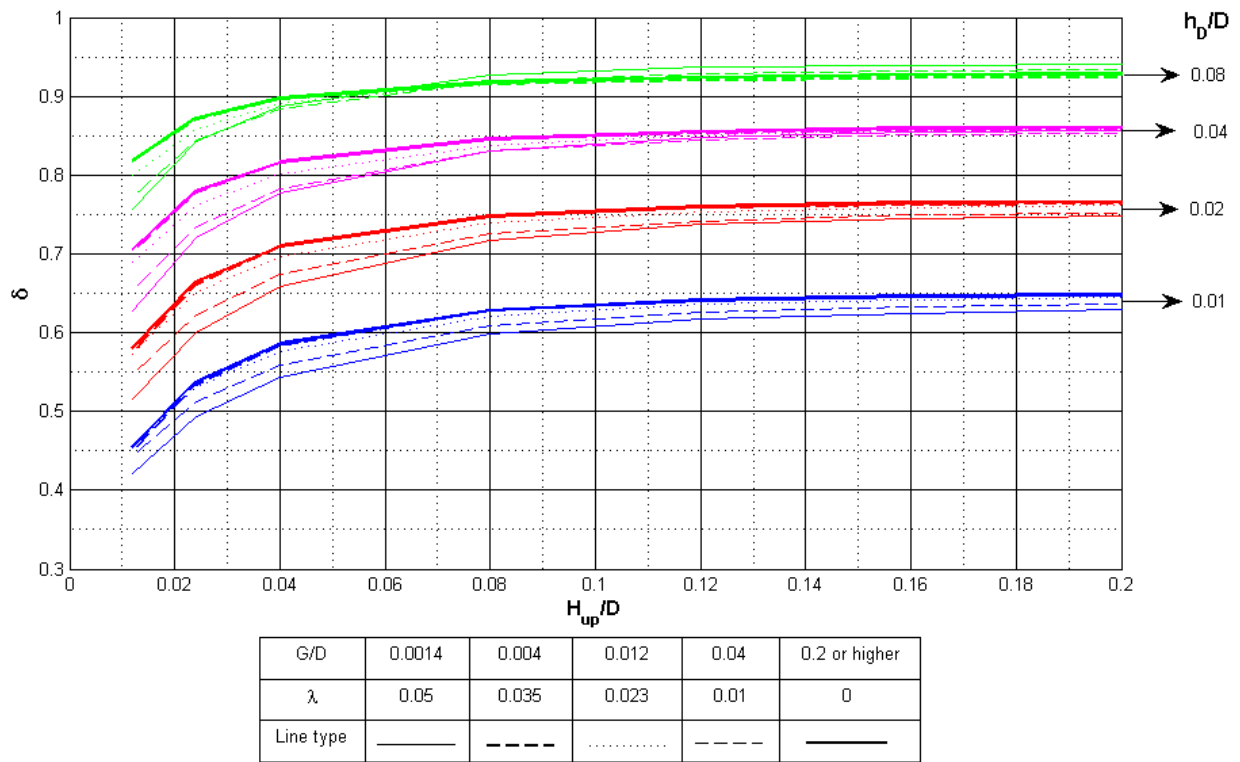


Figure A4. Added mass factor. (4,0) mode-shape.

A2 Fluid added mass. ψ factor.

A.2.1. (1,0) mode-shape

$$\psi = A \cdot (\rho_f / \rho_D)^2 + B \cdot (\rho_f / \rho_D) + C$$

Table A1. Value of equation parameters. (1,0) mode-shape.

$h_D/D = 0.04$															
G/D	0.0014			0.004			0.012			0.04			0.20		
H_{up}/D	A	B	C	A	B	C	A	B	C	A	B	C	A	B	C
0.012	14.90	-9.55	2.08	12.74	-8.35	1.95	10.75	-7.24	1.82	9.62	-6.59	1.75	9.29	-6.40	1.72
0.024	13.08	-8.54	1.96	11.04	-7.40	1.84	8.83	-6.14	1.69	7.25	-5.23	1.59	6.72	-4.92	1.56
0.04	11.50	-7.66	1.87	9.76	-6.68	1.76	7.69	-5.49	1.62	5.97	-4.48	1.51	5.27	-4.06	1.46
0.08	9.25	-6.38	1.72	8.00	-5.67	1.64	6.39	-4.72	1.53	4.81	-3.78	1.43	3.93	-3.23	1.37
0.12	8.06	-5.70	1.64	7.07	-5.12	1.58	5.73	-4.33	1.49	4.36	-3.50	1.40	3.44	-2.92	1.33
0.16	7.35	-5.29	1.60	6.49	-4.78	1.54	5.32	-4.08	1.46	4.10	-3.33	1.38	3.22	-2.78	1.32
0.2	6.89	-5.02	1.57	6.11	-4.56	1.52	5.04	-3.92	1.44	3.93	-3.23	1.37	3.09	-2.70	1.31
$h_D/D = 0.02$															
G/D	0.0014			0.004			0.012			0.04			0.20		
H_{up}/D	A	B	C	A	B	C	A	B	C	A	B	C	A	B	C
0.012	16.51	-10.44	2.18	14.86	-9.53	2.08	13.58	-8.82	2.00	12.93	-8.46	1.96	12.75	-8.36	1.95
0.024	15.16	-9.70	2.10	13.29	-8.66	1.98	11.57	-7.70	1.87	10.43	-7.06	1.80	10.06	-6.85	1.77
0.04	13.99	-9.05	2.03	12.20	-8.05	1.91	10.38	-7.03	1.80	8.95	-6.21	1.70	8.37	-5.88	1.66
0.08	12.17	-8.04	1.91	10.68	-7.20	1.81	9.06	-6.27	1.71	7.55	-5.40	1.61	6.67	-4.89	1.55
0.12	11.12	-7.44	1.84	9.82	-6.71	1.76	8.40	-5.90	1.67	7.00	-5.83	1.57	6.03	-4.51	1.51
0.16	10.51	-7.07	1.80	9.28	-6.40	1.72	7.98	-5.65	1.64	6.70	-4.90	1.55	5.73	-4.32	1.49
0.2	10.00	-6.81	1.77	8.90	-6.18	1.70	7.68	-5.48	1.62	6.50	-4.79	1.54	5.56	-4.23	1.48
$h_D/D = 0.01$															
G/D	0.0014			0.004			0.012			0.04			0.20		
H_{up}/D	A	B	C	A	B	C	A	B	C	A	B	C	A	B	C
0.012	17.90	-11.20	2.27	16.94	-10.68	2.21	16.28	-10.32	2.17	15.95	-10.31	2.15	15.82	-10.06	2.14
0.024	16.86	-10.63	2.20	15.57	-9.92	2.12	14.50	-9.33	2.06	13.76	-8.92	2.01	13.49	-8.77	2.00
0.04	16.03	-10.18	2.15	14.57	-9.42	2.07	13.40	-8.72	1.99	12.32	-8.12	1.92	11.85	-7.85	1.89
0.08	14.70	-9.44	2.07	13.41	-8.73	1.99	12.15	-8.02	1.91	10.87	-7.30	1.83	10.05	-6.85	1.77
0.12	13.89	-9.00	2.02	12.70	-8.33	1.94	11.53	-7.68	1.87	10.30	-6.98	1.79	9.33	-6.43	1.73
0.16	13.35	-8.70	1.98	12.23	-8.07	1.91	11.14	-7.46	1.84	9.96	-6.80	1.77	8.98	-6.23	1.70
0.2	12.97	-8.48	1.96	11.89	-7.88	1.90	10.86	-7.30	1.83	9.77	-6.68	1.75	8.79	-6.12	1.70
$h_D/D = 0.08$															
G/D	0.0014			0.004			0.012			0.04			0.20		
H_{up}/D	A	B	C	A	B	C	A	B	C	A	B	C	A	B	C
0.012	12.80	-8.39	1.95	10.60	-7.15	1.81	8.18	-5.77	1.65	6.57	-4.83	1.55	6.04	-4.51	1.51
0.024	10.42	-7.05	1.80	8.70	-6.07	1.69	6.49	-4.78	1.54	4.69	-3.70	1.42	3.99	-2.27	1.37
0.04	8.52	-5.97	1.67	7.26	-5.23	1.59	5.44	-4.16	1.47	3.73	-3.11	1.35	2.94	2.60	1.30
0.08	6.16	-4.59	1.52	5.40	-4.13	1.47	4.20	-3.40	1.38	2.86	-2.54	1.29	2.04	2.00	1.23
0.12	5.06	-3.93	1.44	4.51	-3.59	1.40	3.59	-3.01	1.34	2.50	-2.31	1.26	1.73	-1.77	1.20
0.16	4.45	-3.55	1.40	3.99	-3.27	1.37	3.23	-2.78	1.31	2.30	-2.17	1.25	1.59	-1.67	1.19
0.2	4.07	-3.32	1.38	3.67	-3.07	1.35	3.00	-2.63	1.30	2.17	-2.08	1.24	1.52	-1.61	1.19

A.2.2. (2,0) mode-shape

$$\psi = A \cdot (\rho_f/\rho_D)^2 + B \cdot (\rho_f/\rho_D) + C$$

Table A2. Value of equation parameters. (2,0) mode-shape.

$h_D/D = 0.04$															
G/D	0.0014			0.004			0.012			0.04			0.20		
H_{up}/D	A	B	C	A	B	C	A	B	C	A	B	C	A	B	C
0.012	11.51	-7.66	1.87	9.79	-6.69	1.76	8.14	-5.75	1.65	7.19	-5.19	1.59	6.94	-5.04	1.57
0.024	9.03	-6.25	1.71	7.71	-5.49	1.62	6.19	-4.60	1.52	5.08	-3.94	1.45	4.73	-3.73	1.42
0.04	7.26	-5.23	1.59	6.29	-4.66	1.53	5.06	-3.93	1.44	4.00	-3.27	1.37	3.59	-3.02	1.34
0.08	5.30	-4.07	1.46	4.70	-3.71	1.42	3.88	-3.20	1.36	3.06	-2.68	1.30	2.63	-2.39	1.27
0.12	4.51	-3.59	1.40	4.04	-3.30	1.37	3.39	-2.89	1.33	2.73	-2.46	1.28	2.32	-2.19	1.25
0.16	4.12	-3.35	1.38	3.71	-3.09	1.35	3.14	-2.73	1.31	2.55	-2.34	1.27	2.19	-2.10	1.24
0.2	3.91	-3.21	1.36	3.52	-2.97	1.34	3.00	-2.63	1.30	2.46	-2.28	1.26	1.26	-1.59	1.18
$h_D/D = 0.02$															
G/D	0.0014			0.004			0.012			0.04			0.20		
H_{up}/D	A	B	C	A	B	C	A	B	C	A	B	C	A	B	C
0.012	14.02	-9.06	2.03	12.43	-8.18	1.93	11.19	-7.48	1.85	10.57	-7.13	1.81	10.41	-7.07	1.80
0.024	11.94	-7.90	1.89	10.42	-7.05	1.80	9.00	-6.24	1.71	8.07	-5.70	1.65	7.80	-5.55	1.63
0.04	10.32	-7.00	1.79	9.04	-6.26	1.71	7.72	-5.50	1.62	6.70	-4.90	1.55	6.31	-4.67	1.53
0.08	8.30	-5.84	1.66	7.37	-5.30	1.60	6.36	-4.70	1.53	5.43	-4.15	1.47	4.95	-3.86	1.44
0.12	7.40	-5.32	1.60	6.62	-4.86	1.55	5.77	-4.35	1.49	4.98	-3.88	1.44	4.49	-3.58	1.41
0.16	6.93	-5.04	1.57	6.23	-4.63	1.52	5.46	-4.17	1.47	4.74	-3.73	1.42	4.30	-3.46	1.39
0.2	6.66	-4.88	1.55	6.00	-4.49	1.51	5.27	-4.05	1.46	4.62	-3.66	1.41	2.57	-2.54	1.29
$h_D/D = 0.01$															
G/D	0.0014			0.004			0.012			0.04			0.20		
H_{up}/D	A	B	C	A	B	C	A	B	C	A	B	C	A	B	C
0.012	16.12	-10.23	2.16	15.06	-9.64	2.09	14.33	-9.24	2.04	13.97	-9.04	2.02	13.85	-8.97	2.02
0.024	14.48	-9.32	2.06	13.23	-8.63	1.98	12.21	-8.06	1.91	11.53	-7.67	1.87	11.30	-7.54	1.85
0.04	13.17	-8.59	1.97	11.99	-7.93	1.98	10.91	-7.32	1.83	10.02	-6.82	1.77	9.68	-6.63	1.75
0.08	11.41	-7.60	1.86	10.42	-7.05	1.80	4.49	-6.52	1.74	8.59	-6.00	1.68	8.08	-5.71	1.65
0.12	10.55	-7.12	1.81	9.67	-6.62	1.75	8.86	-6.16	1.70	8.06	-5.70	1.64	7.51	-5.38	1.61
0.16	10.08	-6.86	1.78	9.27	-6.39	1.72	8.52	-5.96	1.67	7.78	-5.54	1.62	7.27	-5.24	1.59
0.2	9.81	-6.70	1.76	9.02	-6.25	1.71	8.31	-5.84	1.66	7.64	-5.46	1.62	7.16	-5.17	1.59
$h_D/D = 0.08$															
G/D	0.0014			0.004			0.012			0.04			0.20		
H_{up}/D	A	B	C	A	B	C	A	B	C	A	B	C	A	B	C
0.012	8.47	-5.94	1.67	7.09	-5.14	1.58	5.46	-4.17	1.47	4.34	-3.48	1.39	3.98	-3.26	1.37
0.024	5.90	-4.43	1.50	5.06	-3.93	1.44	3.88	-3.20	1.36	2.84	-2.53	1.29	2.45	-2.27	1.26
0.04	4.31	-3.47	1.39	3.79	-3.14	1.36	2.97	-2.62	1.30	2.12	-2.05	1.23	1.74	-1.78	1.20
0.08	2.79	-2.50	1.28	2.52	-2.32	1.26	2.06	-2.00	1.23	1.51	-1.61	1.19	1.18	-1.36	1.16
0.12	2.25	-2.13	1.24	2.05	-2.00	1.23	1.71	-1.76	1.20	1.29	-1.45	1.17	1.01	-1.22	1.14
0.16	1.99	-1.96	1.22	1.82	-1.84	1.21	1.54	-1.63	1.19	1.18	-1.36	1.16	0.94	-1.16	1.14
0.2	1.86	-1.86	1.21	1.70	-1.75	1.20	1.44	-1.56	1.18	1.13	-1.32	1.15	0.90	-1.13	1.13

A.2.3. (3,0) mode-shape

$$\psi = A \cdot (\rho_f/\rho_D)^2 + B \cdot (\rho_f/\rho_D) + C$$

Table A3. Value of equation parameters. (3,0) mode-shape.

$h_D/D = 0.04$															
G/D	0.0014			0.004			0.012			0.04			0.20		
H_{up}/D	A	B	C	A	B	C	A	B	C	A	B	C	A	B	C
0.012	8.86	-6.16	1.70	7.52	-5.38	1.61	6.17	-4.59	1.52	5.39	-4.13	1.47	5.20	-4.01	1.45
0.024	6.39	-4.72	1.53	5.50	-4.19	1.47	4.42	-3.54	1.40	3.62	-3.03	1.34	3.39	-2.89	1.33
0.04	4.88	-3.82	1.43	4.28	-3.45	1.39	3.48	-2.95	1.33	2.78	-2.49	1.28	2.52	-2.32	1.26
0.08	3.46	-2.93	1.33	3.09	-2.70	1.31	2.59	-2.37	1.27	2.10	-2.03	1.23	1.85	-1.86	1.21
0.12	2.98	-2.62	1.30	2.68	-2.43	1.28	2.28	-2.15	1.25	1.89	-1.88	1.21	1.66	-1.72	1.20
0.16	2.77	-2.49	1.28	2.51	-2.31	1.26	2.14	-2.06	1.23	1.78	-1.80	1.21	1.59	-1.67	1.19
0.2	2.68	-2.42	1.28	2.42	-2.25	1.26	2.07	-2.01	1.23	1.74	-1.77	1.20	1.56	-1.65	1.19
$h_D/D = 0.02$															
G/D	0.0014			0.004			0.012			0.04			0.20		
H_{up}/D	A	B	C	A	B	C	A	B	C	A	B	C	A	B	C
0.012	11.79	-7.82	1.85	10.35	-7.01	1.79	9.18	-6.34	1.72	8.61	-6.02	1.68	8.48	-5.94	1.67
0.024	9.44	-6.49	1.73	8.22	-5.79	1.66	7.05	-5.11	1.58	6.30	-4.67	1.53	6.10	-4.55	1.51
0.04	7.82	-5.56	1.67	6.87	-5.01	1.57	5.87	-4.42	1.50	5.10	-3.95	1.45	4.85	-3.80	1.43
0.08	6.10	-4.55	1.51	5.44	-4.16	1.47	4.72	-3.72	1.42	4.10	-3.34	1.38	3.81	-3.15	1.36
0.12	5.46	-4.47	1.47	4.90	-3.83	1.43	4.30	-3.46	1.39	3.78	-3.13	1.36	3.49	-2.96	1.34
0.16	5.18	-4.00	1.45	4.67	-3.68	1.42	4.11	-3.34	1.38	3.63	-3.04	1.34	3.38	-2.88	1.32
0.2	5.04	-3.92	1.44	4.54	-3.61	1.41	1.01	-3.28	1.37	3.56	-3.00	1.34	3.33	-2.85	1.32
$h_D/D = 0.01$															
G/D	0.0014			0.004			0.012			0.04			0.20		
H_{up}/D	A	B	C	A	B	C	A	B	C	A	B	C	A	B	C
0.012	14.39	-9.27	2.05	13.28	-8.66	1.98	10.52	-8.23	1.93	12.16	-8.03	1.91	12.05	-7.97	1.90
0.024	12.38	-8.15	1.62	11.22	-7.50	1.85	10.28	-6.97	1.79	9.66	-6.62	1.75	9.47	-6.51	1.74
0.04	10.90	-7.32	1.83	9.89	-6.75	1.76	8.97	-6.22	1.70	8.24	-5.81	1.66	7.98	-5.65	1.64
0.08	9.18	-6.34	1.72	8.38	-5.89	1.67	7.65	-5.46	1.62	6.99	-5.08	1.57	6.65	-4.88	1.55
0.12	8.50	-5.95	1.67	7.78	-5.54	1.63	7.15	-5.17	1.58	6.85	-4.84	1.55	6.23	-4.63	1.52
0.16	8.18	-5.77	1.65	7.51	-5.38	1.61	6.92	-5.03	1.57	6.38	-4.72	1.53	6.08	-4.54	1.51
0.2	8.02	-5.68	1.64	7.36	-5.29	1.60	6.79	-4.96	1.56	6.30	-4.67	1.53	6.01	-4.50	1.51
$h_D/D = 0.08$															
G/D	0.0014			0.004			0.012			0.04			0.20		
H_{up}/D	A	B	C	A	B	C	A	B	C	A	B	C	A	B	C
0.012	5.67	-4.29	1.49	4.78	-3.75	1.42	3.67	-3.07	1.35	2.88	-2.56	1.29	2.65	-2.41	1.27
0.024	3.55	-3.00	1.34	3.08	-2.69	1.31	2.40	-2.25	1.25	1.77	-1.80	1.21	1.54	-1.64	1.19
0.04	2.44	-2.27	1.26	2.17	-2.08	1.24	1.74	-1.78	1.20	1.28	-1.43	1.17	1.07	-1.28	1.15
0.08	1.54	-1.63	1.19	1.40	-1.53	1.18	1.17	-1.35	1.16	0.89	-1.13	1.13	0.73	-1.00	1.12
0.12	1.27	-1.43	1.16	1.16	-1.34	1.16	0.98	-1.20	1.14	0.77	-1.03	1.12	0.64	-0.91	1.11
0.16	1.16	-1.34	1.16	1.06	-1.27	1.15	0.90	-1.14	1.13	0.72	-0.98	1.11	0.61	-0.88	1.10
0.2	1.11	-1.30	1.15	1.01	-1.23	1.14	0.87	-1.11	1.13	0.69	-0.96	1.11	0.59	-0.86	1.10

A.2.4. (4,0) mode-shape

$$\psi = A \cdot (\rho_f/\rho_D)^2 + B \cdot (\rho_f/\rho_D) + C$$

Table A4. Value of equations parameters. (4,0) mode-shape.

$h_D/D = 0.04$															
G/D	0.0014			0.004			0.012			0.04			0.20		
H_{up}/D	A	B	C	A	B	C	A	B	C	A	B	C	A	B	C
0.012	6.84	-5.00	1.56	5.80	-4.38	1.49	4.73	-3.72	1.42	4.09	-3.34	1.38	3.95	-3.25	1.37
0.024	4.64	-3.67	1.42	4.01	-3.28	1.37	3.23	-2.79	1.32	2.76	-2.47	1.28	2.66	-2.40	1.27
0.04	3.43	-2.92	1.33	3.025	-2.65	1.30	2.48	-2.29	1.26	2.00	-1.96	1.22	1.83	-1.85	1.21
0.08	2.43	-2.26	1.26	2.18	-2.09	1.24	1.84	-1.85	1.21	1.52	-1.62	1.19	1.37	-1.51	1.17
0.12	2.14	-2.06	1.24	1.93	-1.91	1.22	1.65	-1.71	1.20	1.38	-1.51	1.17	1.25	-1.42	1.16
0.16	2.03	-1.98	1.23	1.84	-1.85	1.21	1.57	-1.66	1.19	1.32	-1.47	1.17	1.21	-1.39	1.16
0.2	1.99	-1.95	1.22	1.80	-1.82	1.21	1.54	-1.63	1.19	1.30	-1.46	1.17	1.20	-1.38	1.16
$h_D/D = 0.02$															
G/D	0.0014			0.004			0.012			0.04			0.20		
H_{up}/D	A	B	C	A	B	C	A	B	C	A	B	C	A	B	C
0.012	9.90	-6.75	1.76	8.62	-6.02	1.68	7.56	-5.41	1.61	7.06	-5.12	1.58	6.95	-5.05	1.57
0.024	7.54	-5.40	1.61	6.56	-4.82	1.55	5.60	-4.26	1.48	4.99	-3.89	1.44	4.84	-3.80	1.43
0.04	6.07	-4.54	1.51	5.35	-4.10	1.46	4.58	-3.63	1.41	4.00	-3.27	1.37	3.82	-3.16	1.36
0.08	4.71	-3.71	1.42	4.21	-3.40	1.39	3.67	-3.06	1.35	3.22	-2.78	1.32	3.03	-2.66	1.30
0.12	4.28	-3.45	1.39	3.84	-3.17	1.36	3.37	-2.88	1.33	3.00	-2.64	1.30	2.82	-2.52	1.29
0.16	4.11	-3.34	1.38	3.70	-3.08	1.35	3.26	-2.80	1.32	2.91	-2.58	1.29	2.75	-2.48	1.28
0.2	4.04	-3.30	1.37	3.63	-3.04	1.35	3.20	-2.77	1.31	2.87	-2.56	1.29	2.73	-2.46	1.28
$h_D/D = 0.01$															
G/D	0.0014			0.004			0.012			0.04			0.20		
H_{up}/D	A	B	C	A	B	C	A	B	C	A	B	C	A	B	C
0.012	12.79	-8.38	1.95	11.69	-7.76	1.88	10.93	-7.34	1.83	10.58	-7.14	1.81	10.57	-7.08	1.80
0.024	10.59	-7.15	1.81	9.55	-6.56	1.74	8.70	-6.07	1.68	8.16	-5.76	1.65	8.00	-5.67	1.64
0.04	9.12	-6.31	1.71	8.25	-5.81	1.66	7.48	-5.36	1.61	6.89	-5.02	1.57	6.68	-4.89	1.55
0.08	7.61	-5.44	1.62	6.94	-5.05	1.57	6.34	-4.70	1.53	5.84	-4.40	1.50	5.60	-4.25	1.48
0.12	7.10	-5.14	1.58	6.49	-4.78	1.54	5.97	-4.47	1.51	5.54	-4.22	1.48	5.29	-4.07	1.46
0.16	6.90	-5.02	1.57	6.32	-4.68	1.53	5.82	-4.38	1.50	5.41	-4.14	1.47	5.20	-4.01	1.45
0.2	6.81	-4.97	1.56	6.23	-4.63	1.52	5.75	-4.34	1.49	5.37	-4.11	1.47	5.17	-4.00	1.45
$h_D/D = 0.08$															
G/D	0.0014			0.004			0.012			0.04			0.20		
H_{up}/D	A	B	C	A	B	C	A	B	C	A	B	C	A	B	C
0.012	3.84	-3.18	1.36	3.25	-2.80	1.32	2.50	-2.31	1.26	1.96	-1.94	1.22	1.80	-1.83	1.21
0.024	2.23	-2.12	1.24	1.82	-1.86	1.22	1.53	-1.63	1.19	1.14	-1.33	1.15	1.01	-1.23	1.14
0.04	1.43	-1.55	1.18	1.30	-1.45	1.17	1.02	-1.24	1.14	0.94	-1.13	1.13	0.82	-1.01	1.11
0.08	0.80	-1.07	1.12	0.75	-1.02	1.12	0.60	-0.90	1.10	0.57	-0.85	1.10	0.49	-0.77	1.09
0.12	0.63	-0.94	1.10	0.60	-0.90	1.10	0.49	-0.80	1.09	0.51	-0.78	1.09	0.44	-0.71	1.08
0.16	0.61	-0.90	1.10	0.55	-0.86	1.10	0.45	-0.77	1.09	0.48	-0.76	1.09	0.42	-0.70	1.08
0.2	0.60	-0.89	1.10	0.53	-0.84	1.09	0.43	-0.75	1.08	0.47	-0.75	1.09	0.41	-0.69	1.08

A3 Dimensionless acoustic natural frequency.

The slope (m) of the lines which represents the acoustic mode-shapes in Figure A5 can be calculated as follows:

$$m = \frac{fD/c_0}{c/c_0} = fD/c \quad (16)$$

Combining Eq. (16) with Eq. (17), it is observed that this slope is just a function of the parameter tabulated in Table 4 divided by π for global modes ($k=0$) (Eq. (17)).

$$fD/c = \lambda_i/\pi = m \quad (17)$$

This fact allows to plot that line without performing any simulation, only using Eq. (15) and Table 4. The ratio c/c_0 for which the structural natural frequency will be affected by the acoustic natural frequencies of the fluid cavity can be obtained by using Figure A5 for any kind of disk.

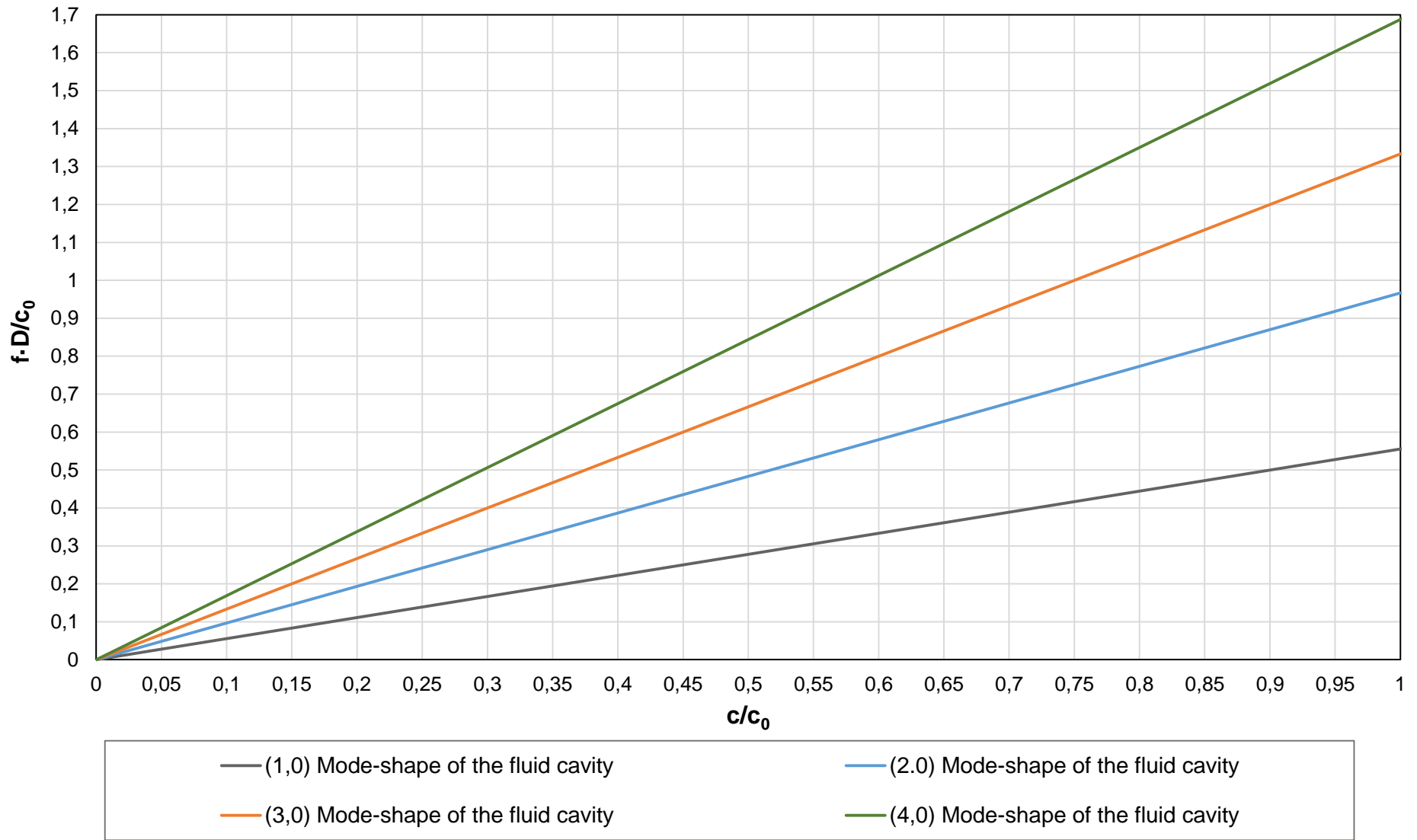


Figure A5. Dimensionless acoustic natural frequency for different c/c_0 values.